Oxidation Behavior of Nanostructured CoNiCrAlY and NiCoCrAlY Sprayed by HVOF

by

Dominic Mercier

A thesis Submitted to the Faculty of Graduate Studies and Research in Partial Fulfillment of the Requirements for the Degree of Master of Engineering

Department of Mining and Materials Engineering

McGill University

Montreal, Canada

February 2010

Foreword

I would like to express my sincere gratitude to Prof. Mathieu Brochu (McGill University) for his support, supervision and patience throughout the course of my research and for his help in the writing of both manuscripts. I'd also like to thank George Kim of Perpetual Technologies™ for his contribution to Chapter 2 as G. Kim provided the CoNiCrAlY coatings. I would also like to thank Bryan D. Gauntt (The Pennsylvania State University) for the transmission electron microscopy work he performed for Chapter 3.

Abstract

In recent years, much development has been made in the world of nanotechnologies. Hence, nanomaterials, which possess unique characteristics and excellent mechanical properties, are now being used in innovative and advanced applications. Despite the incredible potential of nanomaterials, their use is still at an embryonic stage as a result of the difficulty to mass-produce them. Among the potentially viable application remains the fabrication of nanostructured powders to produce high temperature oxidation resistance coatings.

Nanostructured coatings were obtained by thermally spraying cryomilled CoNiCrAlY and NiCoCrAlY feedstock using the HVOF technique. It was found that the milling process used to prepare the powder significantly altered the microstructure of the alloy. In addition to achieving grain size refinement, significant aluminum segregation at grain boundaries was observed. Upon oxidation experiments up to 96 hours in static air at 1000°C an oxide scale composed of an adherent and dense α-Al_2O_3 inner layer with a top layer of fast growing oxides such as NiO, Cr_2O_3, $CoAl_2O_4$ and $NiAl_2O_4$ evolved from the coatings. It was found that the formation of a two-layer scale could be prevented through surface grinding prior to oxidation. Moreover, the comparison of the oxidation results of the powders and those of the coatings revealed that the spraying process has a considerable influence on the oxidation behavior of MCrAlYs attributable to the formation of oxide seeds during the spraying process.

Résumé

Au cours des dernières années, plusieurs avancements ont vu le jour au niveau des nanotechnologies. L'émergence des métaux nanostructurés, possédant des charactéristiques inédites ainsi que des propriétés méchaniques amplement supérieures à celles des métaux conventionnels, a contribuée à leur utilisation pour de nouvelles applications. Malgré le potentiel immense de la nanotechnologie dans le monde des matériaux, l'utilisation de ces maérieux est encore limitée dû à la difficulté de les produire à grande échelle. Cependant, l'une de ces utilisations prometteuses consiste en le développement de poudre nanostructurée destinée à la production de revêtements résistant à l'oxidation à haute temperature.

Le comportement de revêtements nanostructués obtenus par projection thermique à partir de poudres de CoNiCrAlY et de NiCoCrAlY broyées cryogéniquement a été étudié dans un atmosphère oxidant. Il a été démontré que l'étape de broyage modifie considérablement la microstructure des poudres; en plus de réduire la taille de grain, le broyage a mené à une ségrégation de l'aluminum aux joints de grains. Cela a eu pour effet de favoriser la croissance d'une couche protectrice de α-Al_2O_3, bien adhérée et de bonne qualité lorsque les revêtemens ont été oxidés à une température de 1000°C pour des périodes allant jusqu'à 96 heures. Une seconde couche d'oxides à croissance rapide tels que NiO, Cr_2O_3, $CoAl_2O_4$ and $NiAl_2O_4$ a également été observée. Par contre, il a été démontré que cette dernière ne croît pas si la surface des revêtements est polie avant l'oxidation. De plus, en comparant les résultats des tests d'oxidation des poudres avec ceux des revêtements il a été

démontré que la simple projection thermique des poudres influence les résultats d'oxidation due à la formation d'oxides durant la projection.

Acknowledgements

I would like to thank Imperial Oil for their funding of the project and McGill University for their financial support through both my undergraduate and graduate degree at this university.

I would also like to thank the very helpful support staff of the Materials Engineering department, especially Helen Campbell, Monique Riendeau, Robert Paquette, Ray Langlois, Florence Paray and Barbara Hanley. Their support with my many experiments and tests as well as the day to day chats we had truly made my experience in the Master program easier.

I am also grateful to David, David, Patrick, Nicolas, Ramona, Cecile, Renaud, Andreas, Pantcho, Abdulaziz, Yaneth, Graeme, Florencia, Paula, Max, Lydia, Dominique for being there whenever I needed support. Moreover, I would like to thank Cory Kaplin and Jason Milligan for all their assistance with the research as well as their help in the reviewing of this thesis. Finally, I would like to thank my family and friends who supported me and endured me during my time at McGill University.

Table of Contents

List of Figures

List of Tables

Chapter 1. *Introduction*

For the last 30 years, the majority of technological improvements, from electronics to transportation, have been made possible by the development of new materials. Continuing research in the fields of materials science and engineering is focused not only on developing these materials with novel properties but also finding ways to produce more economical alternatives for various applications. Researchers are trying to tailor both the physical and mechanical properties of materials for specific uses. Although there are plenty of new possibilities for the development of special materials, the theory behind micron-size material properties has matured and is well understood. However, the situation is different when investigating materials on the nano-scale. The topic of nanoscale was brought forward during R P Feynman's famous talk *"There is plenty of room at the bottom"* (Feynman 1959). In spite of this, serious research only started 20 years later with the development of the scanning tunnelling microscope (STM) by IBM labs, followed by the atomic force microscope (AFM) and the magnetic force microscope (MFM) which provided researchers with adequate analytical tools to pursue their research. Since then, a large library of scientific papers about nanotechnology has been developed. Potential applications of these materials include: devices for drug delivery systems, semiconductors for solar cell applications, coatings with enhanced oxidation, corrosion and wear resistance as well as structural materials with superior strength to weight ratio, which is especially important in the transportation industry.

1.1 What are Nanomaterials?

Materials are classified in the nanomaterials category when their structure or substructure is on the nanoscale, namely between 1-100nm[1, 2]. Although this refers to a small scale, it is not the potential of miniaturization that opens eyes towards nanotechnology research but rather the novel and surprising electrical[3], mechanical[4-17], physical[18, 19], thermal[20], biological[21] and chemical properties exhibited by these nanomaterials that generate enthusiasm for their technological potential. In fact, some properties of nanomaterials can be so different compared to their conventional micron size counterpart that new models are being developed to understand this unique behavior[22-24]. Nanomaterials gain their particular physical properties due to the high surface energy, spatial confinement (leading to quantum effects), the possibility of having very few defects [25] and the large fraction of surface atoms. At a grain size of approximately 10 nm, 30% of atoms are located at the grain boundaries of a given material (see Figure 1).

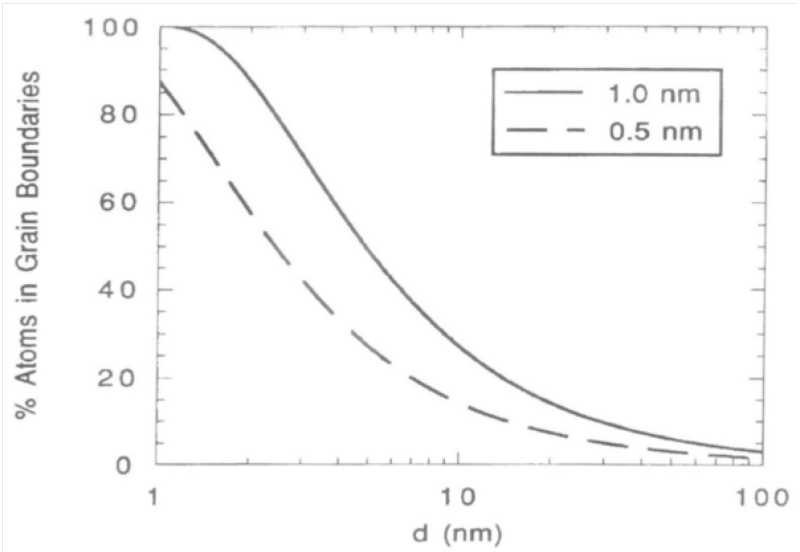

Figure 1: Fraction of atoms at grain boundaries as a function of grain size for a range of grain boundary thickness[26].

Nanomaterials can be divided into two categories: Nanostructured materials which are polycrystalline materials that possess grains that are less than 100nm in at least one dimension and nanoparticles which are individual particles with diameters below 100nm. Nanoparticles can be produced by various techniques such as inert gas condensation[27, 28], sol-gel process[29, 30], cryogenic melting[31, 32], laser ablation[32, 33] and spray pyrolysis[34, 35]. They are often used as drug delivery systems in medicine[36, 37] or as a catalyst due to their high reactivity[38]. Due to their size, nanoparticles can be hazardous to human health and proper precautions must be taken[39]. However, this is not a problem for nanostructured materials due to their larger size.

There are two general approaches to producing bulk nanostructured materials: The "bottom up approach" and the "top down approach", each producing different types of bulk nanostructured material. In the "bottom up approach", individual building blocks such as nanoparticles or individual atoms are assembled together to form the desired part or structure. These can result in very precise structures as each atom can be positioned where it maximizes a specific property. Very high quality products can also be produced through combining powder metallurgy and nanoparticles. The very fast self diffusion of nanoparticles, which was measured to be up to 16 orders of magnitude faster than lattice diffusion for copper with a grain size of 8nm[40, 41], allows for sintering at lower temperature while maintaining a high quality and defect free material.

On the other hand, the "top down approach" as a concept has been applied for decades and is therefore not confined to nanotechnology. It consists in starting from large-scale conventional micron-size materials and trying to improve the hardness and strength by refining the microstructure down to the nanoscale. So far, success in producing nanostructural materials has been limited to the "top down" approach. This is usually obtained via different severe plastic deformation techniques such as equal channel angular pressing, high-pressure torsion, cryogenic milling, etc.[42].

The mechanical strength of nanostructured materials has been a source of confusion as the relationship between their yield strength and grain size is very complicated. Both hardening and softening have been associated with reduction of the grain size into the nano-regime [7, 17, 43]. This can be attributed to a break down of the Hall-Petch relation, which relates the yield strength of materials to the grain size[44], below a certain critical grain size, d_c [45]. This point corresponds to when dislocation pile-up is no longer possible due to the fact that individual grains are too small to accommodate more than one dislocation[46]. Various studies have reported that the increase in the volume fraction of grain boundaries associated with a nano grain size distribution was very effective in hardening the materials as predicted by the classical Hall-Petch equation[6, 12, 14, 47]. Consequently, pure nanostructured materials such as copper and titanium have shown superior strength compared to similar coarse grain and alloyed metals as illustrated in Figure 2 [43]. In fact, Wang et al. have shown that nanocrystalline copper with an average grain size of 30nm can exhibit yield strength up to 760MPa[16]. This particularly

interesting because a large increase in yield strength is normally associated with a dramatic reduction in ductility but this was not the case in Wang's research.

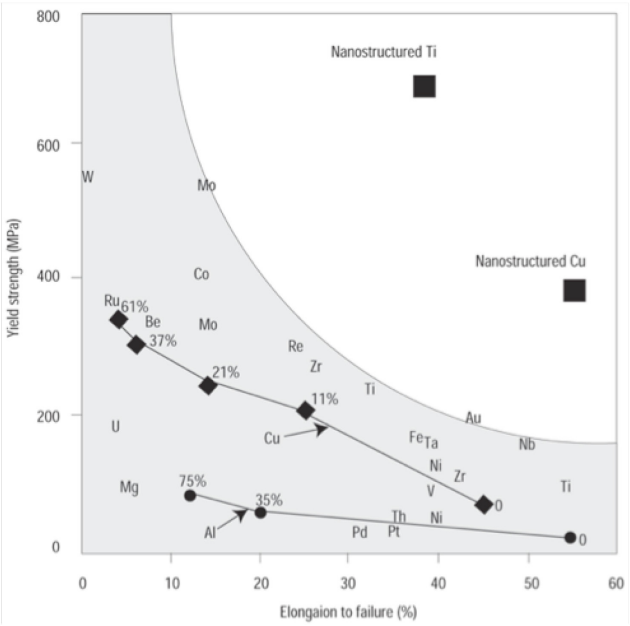

Figure 2: Relation between yield strength and ductility for different copper and aluminum alloys with comparison to nanostructured non-alloyed Ti and Cu[48].

Although the increased strength of nanocrystalline materials is a reason why these materials are good candidates for structural applications, their low ductility and toughness is one of the key-limiting factors to their practical use[4, 8, 49]. However, in recent years much research has been devoted to increasing the ductility of nanostructured materials. In fact, the ductility of nanostructured copper has been greatly increased by using a bimodal grain size distribution[11, 15] and by having low-angle grain boundaries with low grain boundary energy which facilitate grain boundary sliding[9, 10]. Similar observations have been made with aluminum

alloys; Tellkamp et al. increased the yield strength and ultimate tensile strength of commercially available Al 5083 up to 30% without losing ductility when nanostructuring the powder through cryomilling[13]. In addition, Zhang et al. have been able to produce nanostructured Ag having minimal defects with ductility reaching 22%[50, 51].

The potential for nanostructured materials with high yield strength and good ductility in structural applications is endless. The exceptional mechanical properties offered by nanostructured light metals such as aluminum and titanium could fulfill the constant demand of the transportation industry for stronger and lighter materials. Unfortunately, the manufacturing of bulk nanomaterials in large quantity is still difficult. Only a few processes such as cryomilling have shown potential for higher production output, but the product remains expensive. In fact, Ye and Schoenung have evaluated the price of B_4C reinforced nanostructured 5083 aluminum powder to be around $320 USD/kg, much more expensive than pure 5083 powder[52].

1.2 Description of Cryomilling

Many techniques have been developed to create nanostructured powders including gas condensation, crystallization of amorphous alloys, mechanical alloying/milling and electrodeposition [53]. Although they can all produce high quality powders,

only mechanical milling has been able to produce economically viable large quantities of nanostructured powders [53].

Mechanical milling/alloying was initially used to produce alloyed powders and oxide dispersed powders[54]. However, it also has the capability of refining the grain size of powders down to the nano-level[55]. This can be achieved through high-energy input and a controlled milling environment. The process can occur in different types of mills, but the attritor mill is the one most often used for nanostructured powders[53]. An attritor mill consists of an impeller, grinding media (usually 6-7mm stainless steel balls), a double-wall tank and a high power electric motor as described in Figure 3.

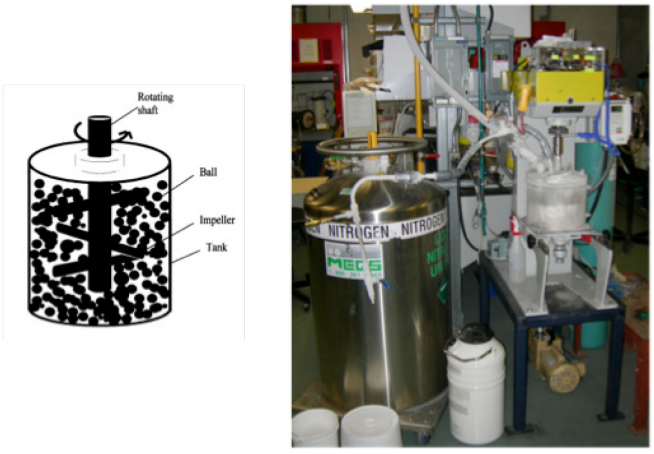

Figure 3: Cryomilling apparatus

The rotational energy of the impeller transferred to the slurry of powder/grinding media causes the powder particles to experience severe plastic deformation leading

to a reduction in grain size[56]. The mechanism for the microstructure refinement [57, 58] is described in Figure 4. Three main steps are proposed: 1) Upon impact by the grinding media, the powder particles are plastically deformed, flattening the particles and increasing their dislocation density, Figure 4b. 2) With increasing milling time, the additional impact energy is stored into shear bands of high dislocations density. At certain localized strain level, it then becomes more favorable for the dislocations to annihilate and realign into sub nano-grain boundaries, Figure 4c, creating a bimodal grain structure. 3) Upon further milling time, the strain level becomes more homogenous and all the sub grain boundaries transform into high angle grain boundaries resulting in nano-scaled grains in the particles. At that point, the flattened particles can no longer accommodate plastic deformation and they start breaking into chips. The broken particles then re-weld together to form granular structures, Figure 4d, [59].

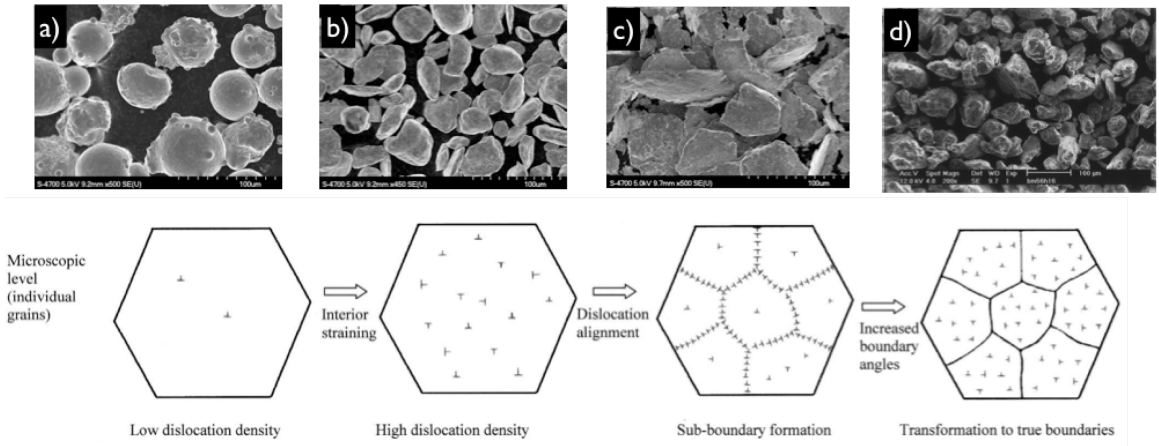

Figure 4: Microstructure refinement of the powder during the milling process. Adapted from[58].

Cryomilling differs from other milling techniques due to the controlled environment and temperature (-196°), provided by liquid nitrogen, at which it is undertaken. Liquid nitrogen is important for the microstructure refinement process because it prevents dynamic recovery of the highly deformed microstructure during milling[60]. Although the high milling energy is sufficient to refine the microstructure, the heat generated during the process would prevent the new grains from staying in the nano-regime. In addition, liquid nitrogen prevents air contamination of the powder. During the milling process, particles are broken exposing fresh surfaces which are susceptible to oxidation. Finally, liquid nitrogen can react with elements such as aluminum to form nitrides which can have a beneficial effect on thermal stability of the powders[61].

1.3 Thermal Stability of Cryomilled Powder

Cryomilled powders have good thermal stability which is an advantage over those prepared by other milling techniques. As these powders are usually used as feedstock for thermal spraying processes[62-64], it is important that the nanostructure be kept after deposition. The thermal stability of cryomilled powder can be attributed to the formation of aluminum nitrides (AlN) during cryomilling[65, 66]. The nitrides segregate at grain boundaries effectively pinning them and limiting their motion at elevated temperature. Kinetic and thermodynamic strategies have been developed to understand the thermal stability

of nanostructured coatings. Both are directly linked to grain boundary segregation[67]. The kinetics approach proposes that the segregation at grain boundaries reduces the grain boundary mobility, *m*. However, *m* is described by an Arrhenius equation and grain growth will eventually happen at high temperature. On the other hand, the thermodynamic approach is not as temperature dependent[68]. The theory stipulates that in systems with high segregation energy it is possible to reduce the grain boundary energy to zero and suppress grain growth[67, 68].

Figure 5 presents results of nanostructured powders that were annealed for 1 hour at different homologous temperatures[57]. It can be observed that the two powders with the better thermal stability were both prepared by cryomilling. Moreover, the addition of aluminum to the alloy proves to have a great impact on impinging grain growth. In fact, the cryomilled Fe powder without aluminum sustained severe grain growth starting at 0.45 of the melting temperature, but only a 2.6% aluminum addition was sufficient to maintain a grain size at around 50nm at a homologous temperature of 0.75.

As described in this section nanomaterials and nanostructured materials offer properties that are unmatched by the conventional coarse grain materials. However, part of the challenge also resides in finding applications where these novel properties can be utilized at a reasonable manufacturing cost. The following sections discuss different combinations of nanomaterials and their applications.

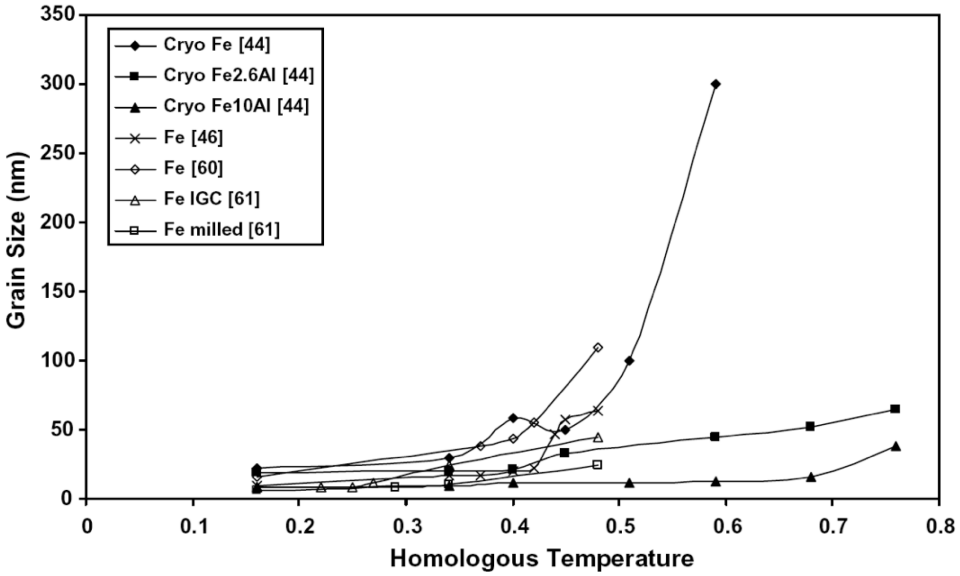

Figure 5: Thermal stability of different nanostructured powders with respect to their homologous temperature[57].

1.4 High Temperature Environment

Many industrial processes such as aircraft gas turbine engines, land-based gas turbines, petroleum refining and nuclear power generation operate in rigorous high temperature environments that demand a lot from their components[69]. In gas turbines, the process efficiency increases with increasing temperature, currently temperatures as high as 1600°C can be reached. In the petroleum industry, the crude oil is catalytically cracked at temperatures sometimes reaching 1000°C by circulating the oil through a series of metallic pipes, resulting in various usable by-products.

The harsh conditions imposed by these processes demand structural materials that can operate under a wide range of mechanical and chemical conditions. These materials must have high temperature strength, good creep resistance and excellent hot oxidation and corrosion resistance in order to maintain the integrity of the components and the efficiency of the processes. The selection of materials for these harsh conditions has always been difficult and the research has focused on developing materials that can maintain their load bearing capabilities such as: fatigue and creep resistance at high temperature; the degradation of the components due to chemical attack being a lower priority. The reason is that an ideal material that can satisfy both design requirements has yet to be developed. Among the different families of materials available for high temperature application presented in Figure 6, nickel-based superalloys are best suited. These alloys normally have up to 6% aluminum for precipitation strengthening and oxidation resistance purposes[70]. However, that aluminum concentration is insufficient to provide complete oxidation resistance. Unfortunately, although increasing the aluminum concentration would result in an increased high temperature oxidation resistance, it would also lower the much needed creep resistance[69]. Hence, to provide resistance to the oxidative and corrosive environment without compromising the mechanical properties, thin metallic coatings have been developed[71].

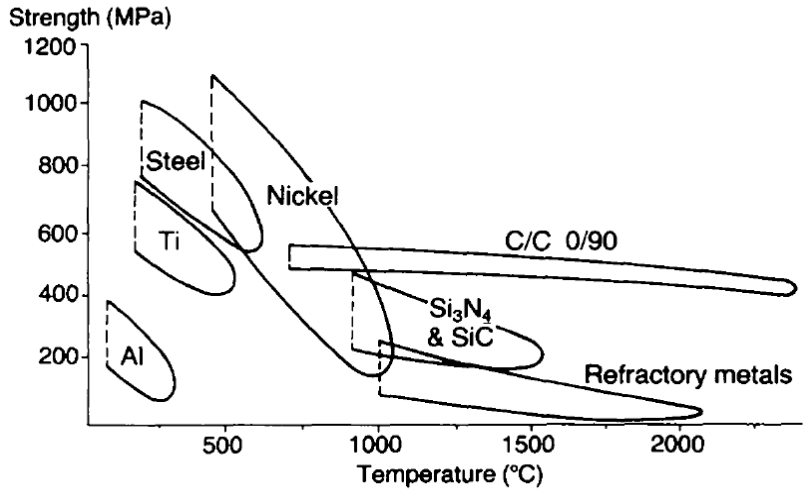

Figure 6: Working temperature range of high temperature materials[72]

1.5 The Use of Coatings

Coatings have been developed to remedy different surface problems such as oxidation, wear and discoloration, and in so doing extending the life of the underlying alloy[71]. In the case of protection against high temperature oxidation, there are a number of requirements that the coating must fulfill. These must offer a protection against oxidation by forming a thermodynamically stable, adherent and slow growing oxide scale and must have a sufficient concentration of the protective scale former, usually aluminum or chromium[69, 73]. The coating must also have a stable microstructure at high temperature, avoiding phase transformation in the working temperature range. Finally, the coating material needs to have a good thermal matchup with the substrate to reduce thermal stresses during heating cycles[74].

1.6 General Oxidation

High temperature coatings for oxidation resistance are developed to promote selective oxidation of specific alloying elements. Thermodynamically, most materials will oxidize at high temperature because their free energy change associated with the reaction is negative. However, not all oxides can offer protection of the substrate. The monoxides NiO and CoO for example will often form in the early oxidation stages on Ni and Co containing alloys, but their fast growth rate and porous structure allow for constant diffusion of oxygen and metallic ions which is detrimental to the base material. Only the oxides of aluminum (Al_2O_3), chromium (Cr_2O_3) and silicon (SiO_2) have been found to offer adequate protection against high temperature oxidation[75]. Hence, the development of high temperature alloys for coatings is such that the selective oxidation of these elements is promoted. However, silicon is not added as an oxide scale former to high temperature coatings but it is rather used to increase the oxide scale adherence. Unfortunately, it was also found to lower the melting point of the coatings[76]. Selective oxidation of aluminum is often favored over chromium because the growth rate constant of Cr_2O_3 is two orders of magnitude higher than that of Al_2O_3, which offers less protection[77]. In addition, the use of Cr_2O_3 as a protective scale is not effective at temperatures above 1000°C as Cr_2O_3 becomes unstable and transforms to the volatile CrO_3 gas; this transformation has even been reported to occur at temperatures as low as 850°C and 900°C[78].

1.7 Materials Selection for Coatings

Two primary types of coatings offering selective oxidation of aluminum have been developed to protect nickel-based superalloys: diffusion coatings and overlay coatings[79, 80]. The diffusion coatings process consists of increasing the surface concentration of a protective oxide-scale former, such as Al, by various techniques including pack cementation[81] and chemical vapor deposition[82] creating "aluminide" coatings. These coatings initially suffered from low adherence of the oxide scale, however, studies have shown that superior resistance to high temperature oxidation was possible with the use of platinum-modified aluminide coatings[83-85]. The reaction between the aluminum/platinum surface layer and the nickel in the superalloy either forms the intermetallic phase β-NiAl, or a mixture of PtAl and $PtAl_2$ in a β-NiAl matrix[86]. The presence of these stable aluminum-containing phases at the surface of the alloy/coating system facilitates the growth of the protective Al_2O_3 scale. Thus, diffusion coatings offer good protection against high-temperature oxidation[87]. However, superior oxidation resistance can be obtained with the use of overlay coatings such as MCrAlYs: this can be observed in Figure 7. The main advantage of MCrAlY overlay coatings is that their chemical composition is independent of the substrate which offers a wider range of possible compositions[88]. As opposed to diffusion coatings, the interaction between the overlay coating materials and the substrate is only to provide bonding and no chemical phase transformation occurs. The most common deposition methods for these coatings are physical vapor deposition (PVD), which include electron beam

physical vapor deposition[89-91], sputtering[92, 93], vacuum arc evaporation[94] and spraying techniques which are preferred for industrial application and include vacuum plasma spray (VPS)[64, 95, 96], air plasma spray (APS)[62, 97, 98] and high velocity oxy-fuel (HVOF)[62, 96, 99-103].

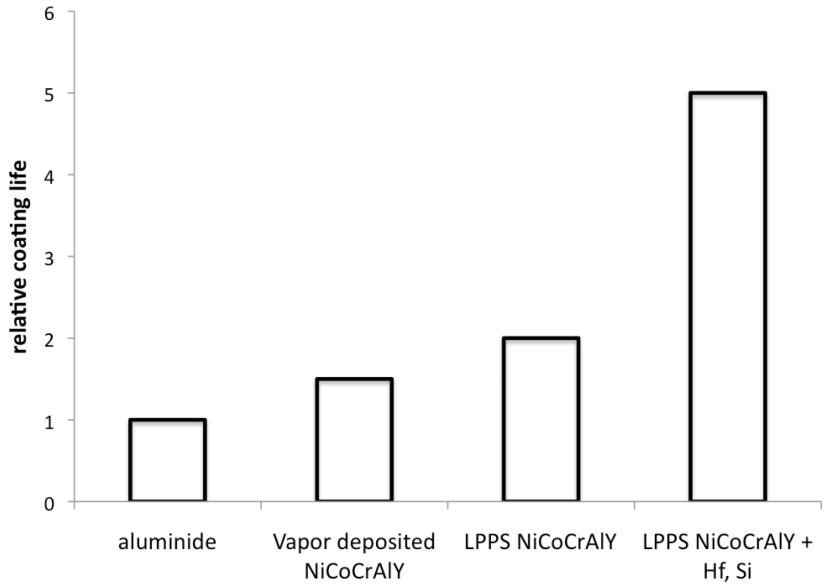

Figure 7: Comparison of the life of different high-temperature coatings in an oxidizing atmosphere[104].

As mentioned above, MCrAlY overlay coatings offer excellent protection against high temperature oxidation and corrosion. MCrAlYs are based on the superalloy system but are designed to offer superior environmental resistance rather than structural support. The increase in resistance is mostly provided by the presence of Y and other alloying elements such as Hf, Ta, Ti, Re and Si which increase the oxidation resistance by improving the oxide scale adherence[105].

The composition of an overlay MCrAlY (M=Ni, Co or both) coatings is based on that of a nickel-based superalloy. The three main alloys used for high temperature oxidation are NiCrAlY, CoNiCrAlY and NiCoCrAlY. The utilization depends on the working environment and the substrate alloy. CoCrAlY can also be used for hot corrosion problems[106]. The microstructure of MCrAlYs is relatively complex due to the presence of many alloying elements. Some major differences when compared to the superalloys are the higher aluminum concentration in MCrAlY alloys, normally between 6 and 12%, for high temperature oxidation resistance[107] and the addition of yttrium which improves the oxide scale adherence[108]. The following phases characterize the microstructure of MCrAlYs[109]:

γ : (Ni, Co) primary phase

γ' : (Ni_3Al) secondary phase

β : (NiAl) Al-rich phase

σ : CoCr

α : Cr

Typical MCrAlYs used in thermal spray such as CoNiCrAlY and NiCoCrAlY are considered to be dual phase alloys consisting of the γ-Ni or Co rich solid solution and the β-NiAl second phase which is rich in aluminum and often referred to as the aluminum reservoir[76]. The second phases σ and α are quite minor and do not generally play an important role in MCrAlYs. However, the γ'-Ni_3Al is present in CoNiCrAlY and NiCoCrAlY as nanometer-sized coherent precipitates and offers

increased mechanical properties[110]. Achar et al. have demonstrated that the addition of Co favors the formation of aluminum rich β-NiAl at high temperature at the expense of the aluminum weak γ'-Ni_3Al[111]. As a result, the microstructure of NiCrAlY is slightly different as the Ni-rich γ and γ'-Ni_3Al are the major phase, β-NiAl phase not being normally present[112].

1.8 Oxidation of MCrAlY

This research has focused mainly on the oxidation behavior of thermally sprayed CoNiCrAlY and NiCoCrAlY coatings, whose complete oxidation behavior is complex. In addition to the protective Al_2O_3 scale, there are a number of other oxides that are thermodynamically favorable to form. In order to predict which oxides forms on the surface of CoNiCrAlY, a thermodynamic model was developed using Factsage™.

The simulation was done for the CoNiCrAlY system and it was assumed that the results would be similar for NiCoCrAlY. Factsage™ predictions only take into account thermodynamic information for its calculation and do not take into consideration process kinetics, which is very important in oxidation processes. However, it gives a good idea of which oxides form under specific conditions. The phase diagram presented in Figure 8 shows which phases are present when CoNiCrAlY is exposed to varying oxygen activity and temperature. The oxygen activity was varied in an attempt to account for the kinetic dependence of oxidation

and to illustrate oxide layering. Hence, at low oxygen activity, the corundum oxide phase composed of Al_2O_3 and Cr_2O_3 is predicted to form, which is in agreement with the literature[113, 114]. As the oxygen activity is increased, different spinels such as $CoAl_2O_4$, $NiAl_2O_4$ and $CoCr_2O_4$ will form followed by the growth of the monoxide phase, NiO and CoO, at higher oxygen activity. It is important to understand that these predictions do not account for the slow diffusion of ions through Al_2O_3[115]. Therefore, it is possible that during the high temperature service of a coating, not all of these oxides form; especially if the Al_2O_3 scale is defect free.

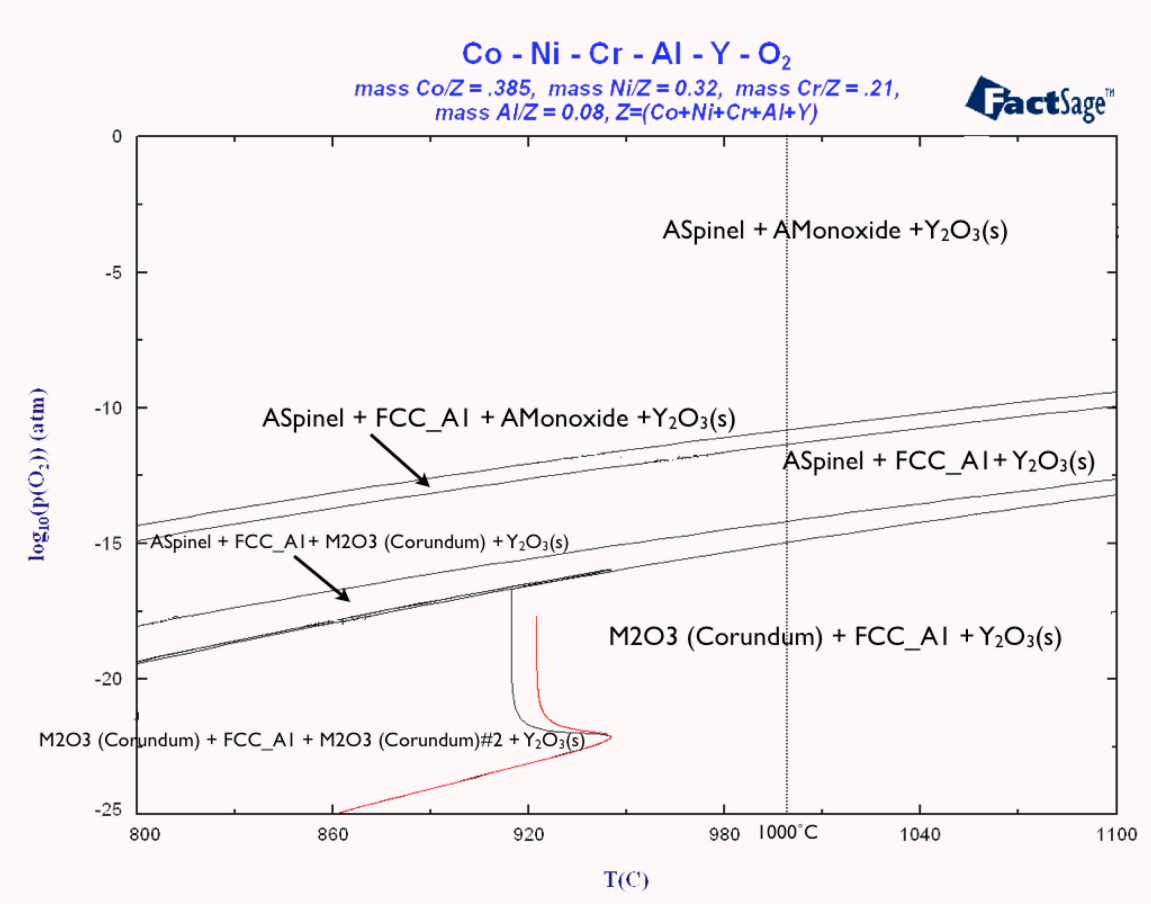

Figure 8: Phase diagram of the CoNiCrAlY system with varying oxygen activity and temperature

Unfortunately, it is very difficult to develop oxidation models that take kinetics into consideration. Nevertheless, it is possible to make good predictions from the several studies conducted on the oxidation of the different MCrAlYs. Pettit et al have studied the effect of the aluminum concentration on the oxidation behavior of the Ni-Al system[116]. It was demonstrated that internal Al_2O_3 forms with external $NiAl_2O_4$ and NiO when the aluminum content is between 1-6 wt%, for Al concentration of 6-17 wt%, external Al_2O_3 forms but the concentration is too low to maintain the supply of Al for long oxidation times at which point a mixture of NiO, $NiAl_2O_4$ and Al_2O_3 develops. The behavior is different for MCrAlY coatings. Firstly, chromium increases the aluminum activity[85] which means that an external Al_2O_3 scale can form at lower Al concentration. Secondly, the rate of aluminum depletion (β-NiAl) decreases with increasing Co content[117] which retards the formation of NiO and $NiAl_2O_4$ due to aluminum depletion.

Chemical breakdown due to aluminum depletion during oxidation is one of reason for the deterioration of the thermally gown oxide (TGO). During the oxidation of MCrAlYs a progressive reduction of the aluminum rich β-NiAl phase occurs to feed the formation of the Al_2O_3 scale. The microstructure then evolves as described in Figure 9, according to the following reactions:

1→ Al-rich β converts to Ni-Rich β

2→ Ni-rich β converts to β+γ'

3→ β+γ' converts to γ'+ γ

4→ γ'+ γ converts to γ

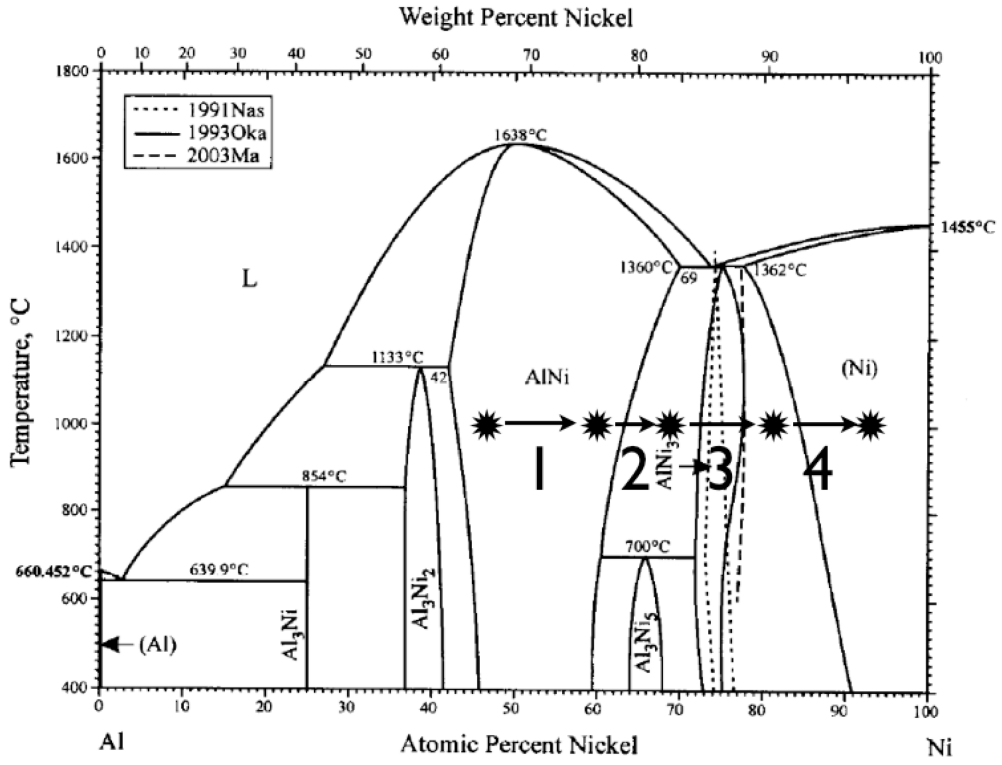

Figure 9: Ni-Al phase diagram[118].

When all the β-phase has been converted in to the primary γ-phase, the aluminum concentration below the TGO/coating interface is not enough to continue the growth of the Al_2O_3 scale. As a result, although diffusion through the Al_2O_3 scale is very slow as mentioned previously, an insufficient concentration in aluminum coupled with defects in the Al_2O_3 scale, causes Ni, Cr and Co ions to diffuse to the surface resulting in the formation of a mixed oxide layer[119]. Ali et al. have reported that α-Cr_2O_3 and the $(Ni,Co)(Cr,Al)_2O_4$ spinel phase start to form when the Al concentration reaches a critical low value[120]. Moreover, they make note of a reduction of the Al_2O_3 scale after aluminum depletion with increasing oxidation time. This can be attributed to the solid state reaction between the NiO and Al_2O_3

oxides which forms $NiAl_2O_4$[121, 122]. Finally, in cases where the Al_2O_3 scale is damaged or has completely disappeared, internal formation of spinels and Cr_2O_3 occurs in the aluminum depleted zone[45].

A remedy to the chemical breakdown previously discussed relies on the use of nanostructured MCrAlY coatings. The increased diffusivity provided by the higher volume fraction of grain boundaries allows for an easier supply of aluminum to the surface even at lower concentration[123]. This allows more time for a sound Al_2O_3 scale to develop. Additionally, the oxide resistance to thermal cycling is greater for nanostructured coatings as the bonding force between the oxide and the coating is directly proportional to the volume fraction of grain boundaries exposed to the surface[124].

1.9 Characterization of Nanostructured Materials

The determination of the grain size is mandatory when performing studies on nanostructured materials. It usually carried out by two techniques: Transmission electron microscopy (TEM) and X-ray diffraction (XRD). XRD has the advantage of scanning a larger area, hence the grain size obtained is more representative. However, it is limited to the grain size measurement of the surface and its accuracy is debatable. On the other hand, the TEM technique is much more precise, but it is limited to a small specific location.

Grain size determination by TEM can be done by two different techniques. The first one consists in obtaining either a dark field or a bright field image (or both) and measuring the grain size using an image analysis software or by manually counting the grains of well defined contours[125]. The second technique consists of measuring the width of the rings on a selected area diffraction (SAD) pattern. The formation of rings on SAD pattern is characteristic of polycrystalline materials and the width of individual rings can be related to the grain size through Equation 1 [126].

$$D = \frac{rd}{\Delta r} \qquad \text{Equation 1}$$

Where, D is the grain size, r is the radius of the ring, d is the interplanar spacing of the respective ring and Δr is the width of the ring. From the equation, it can be seen that the width of the ring is inversely proportional to the grain size. The drawback of this technique is that, although it is theoretically valid and accurate, it fails to give information about the grain size distribution; the thin ring produced by the larger grain is convoluted into the broader ring produced by the smaller grains[127].

The measurement of grain size by XRD is often used for nanostructured materials due to its simpler sample preparation compared to TEM. The method is based on the measurement of the broadening of the diffraction peaks which is primarily caused by two factors: grain size refinement and atomic level microstrain[128]. This method is only valid for materials below 100 nm as

broadening of the diffraction peaks due to an increase in grain boundaries is negligible above 100 nm[129]. There are a number of equations that have been developed to connect peak broadening with small grain size. The simplest of them is the Scherrer equation, Equation 2, which is derived from Bragg's law.

$$D = \frac{k\lambda}{\beta \cos\theta} \qquad \text{Equation 2}$$

where D is the crystallite size, k the shape factor, λ the wavelength of the x-rays, B the width of the peak at half-maximum (FWHM) and θ is the Bragg angle. The Scherrer equation is only accurate for measuring annealed materials because it does not account for microstrain. Therefore, it cannot be used with materials that were produced by severe plastic deformation such as cryomilling. Other equations such as those based on the integral breath analysis are then more appropriate[129-131]. However, it is impossible to use the integral breath analysis when dealing with MCrAlY's subjected to severe plastic deformation as the broadening of the first γ/γ' and β peaks overlap each other, making it impossible to evaluate the broadening of the individual peaks.

1.10 Research Objectives

This is a manuscript-based thesis composed of two manuscripts that have been submitted for publication. Some of the information found in the introduction of this thesis might be repeated in the introduction of both manuscript as their content has not been significantly altered from the version that was submitted for publication.

The main objective of this research has been to develop a stand-alone coating capable of resisting the harsh and oxidative environment found in the high temperature of oil refining boilers. The research has yielded two papers on the oxidation behavior of nanostructured CoNiCrAlY and NiCoCrAlY sprayed by HVOF.

The purpose of Chapter 2 is to demonstrate that stand-alone CoNiCrAlY coatings obtained by nanostructured feedstock offer a better oxidation resistance than those obtained by conventional powder. The oxidation behavior of CoNiCrAlY is well documented. However, most of the research has been focused on its oxidation behavior in the thermal barrier coating (TBC) system and very few studies have concentrated on stand-alone CoNiCrAlY coatings. Moreover, the majority of the publications studying the effect of nanostructure on the oxidation behavior of CoNiCrAlY are devoted to coatings and no research has been done on the nanostructured powders prior to spraying. Therefore, the oxidation behavior of nanostructured coatings and powders will be compared to evaluate the influence of spraying.

Chapter 3 reports the feasibility of using nanostructured NiCoCrAlY powders to produce high temperature oxidation resistant coatings. The improved oxidation resistance obtained by nanostructured coatings is provided by the increase in grain boundary volume fraction. However, the exposure of the material to high temperature, initially during spraying and then during service is expected to modify the grain structure. In this chapter, the thermal stability of nanostructured powders is evaluated.

Chapter 2. Parameters Influencing the Oxidation Behavior of Nanostructured CoNiCrAlY

Dominic Mercier[1], George Kim[2] and Mathieu Brochu[1]

[1]Departement of Materials Engineering, McGill University, Montreal, Qc, Ca

[2]Perpetual Technologies Inc, Montreal, Canada

2.1 INTRODUCTION

Higher combustion temperatures in gas turbines (aero and land-based) result in an increase in efficiency and in a reduction of gas emissions, hence the strive to develop materials that can withstand these harsh conditions is on-going. Currently, the components in the hot zone, such as the combustor, the transition ducts, and the turbine blades, are made of nickel based alloys which cannot maintain strength at temperatures higher than 600-650°C [132]. To increase the operating temperature to around 1000°C, a thermal barrier coating (TBC) is applied on the nickel-based components. The TBC consists of an yttria-partially-stabilized zirconia (YPSZ) top coat and an MCrAlY bond coat. To date the research on MCrAlYs (M=Ni, CoNi or NiCo) has been oriented almost exclusively towards the aerospace applications. They are used as bond coat on which a thermally grown oxide (TGO) protects the nickel-based components against high temperature oxidation.

CoNiCrAlY gains its excellent high temperature oxidation resistance from its ability to grow Cr_2O_3 and Al_2O_3 on its surface when exposed to oxidative conditions. The presence of Co in CoNiCrAlY, as opposed to the NiCrAlY system provides the advantage of increasing the stability of the β-NiAl phase at high temperature[111]. This improved thermal stability is important as the β-phase is the aluminum reservoir for the growth of Al_2O_3. Thus, the improved oxidation resistance of these materials opens them up to applications as stand alone coatings for oxidative atmosphere.

Although MCrAlY alloys were developed many years ago, failure of the coating/TGO system is still often caused by thermo-mechanical mismatch between the coating and the oxide layer. Spallation of the TGO has been linked to the growth of fast growing oxides such as NiO, Cr_2O_3, $NiAl_2O_4$ and other spinels. It is therefore essential to improve the oxidation resistance of CoNiCrAlY coatings by favouring the formation a more protective and adherent oxide such as Al_2O_3. Alumina can grow as different metastable structures such as θ-Al_2O_3, γ-Al_2O_3 and δ-Al_2O_3 on CoNiCrAlY which will eventually transform to the stable corundum α-Al_2O_3 phase[133]. The implications of these transformations on the oxidation behavior are significant. The density of θ-Al_2O_3 being 12% higher than α-Al_2O_3[133]. Also, the growth of each phase follows different transport mechanisms which has an impact on the growth of the whole TGO[134]. As a result α-Al_2O_3 is preferred because the slow diffusion of cations and oxygen through its lattice results in a slow and dense growing oxide[115, 135].

Previous research by Lou et al. showed that the nature of the growing oxide layer is not only dependent on the chemistry of the alloy but can also be altered by the grain size of the deposited coating[136]. They demonstrated that an as-cast K38G superalloy formed a Cr_2O_3 scale while its nanostructured counterpart, obtained by sputtering, formed a Al_2O_3 oxide when oxidized in air at 1000°C. In recent years many studies have proven that nanoscrystallization of the coating improved the oxidation resistance of NiCrAlY [99, 113, 137] and CoNiCrAlY [114, 138].coatings. The improvement in oxidation behavior is mainly attributed to two factors, firstly, nanocrystallization accelerates the formation of a uniform α-Al_2O_3 scale. This behavior is a function of the Al distribution in the deposited coating. For coatings with smaller grain size, the lattice diffusion distance is decreased, and simultaneously the volume fraction of grain boundaries is increased. Taking into account that for both situations, the diffusion coefficient of Al is bigger than for Cr, a uniform transport of Al to the surface can be obtained. Another advantage of reducing the grain size resides in the improved adherence of the scale on the coatings, as reported by Wang F. [124].

MCrAlYs can be deposited by various techniques including vacuum plasma spray (VPS), high frequency pulse detonation (HFPD), electron beam physical vapour deposition (EB-PVD) and high-velocity oxygen fuel (HVOF)[63, 91, 139, 140]. HVOF has been particularly interesting recently because of the ability to spray at atmospheric pressures eliminating the need for special spraying chambers. Moreover, HVOF sprayed coatings possess high density, strong adhesion to

substrates and the relatively low thermal influence during spraying makes possible to maintain crystal structure in the nano-regime[141].

The objective of this study is to investigate the oxidation behavior of nanostructured CoNiCrAlY. Static oxidation tests will be performed on the powder and on the HVOF sprayed coating to evaluate the effect of nanostructure, in-flight oxidation and milling itself. Also, particular attention will be paid to the distribution of aluminum in the nanostructure coating and its influence on the oxidation behavior.

2.2 EXPERIMENTAL PROCEDURE

Commercially available gas atomized Amdry 9951 CoNiCrAlY feedstock (-325 mesh), produced by Sulzer Metco, was used in this study, and the morphology and the particle size distribution can be observed in Figure 10. The composition of the alloy can be found in Table 1. Nanostructure was obtained through cryomilling; a complete description of the technique can be found in Witkin and Lavernia's work [57]. The process parameters used were 16 hours milling in a Union Process 1-S attrition mill at 180rpm, which yielded a flaky morphology, as depicted in Figure 11. Liquid nitrogen was continuously added to the vessel to compensate for evaporation. Stearic acid (0.2%) was added to the powder as process control agent to prevent particles from coating the steel balls and the vessel. The ball to powder ratio was 30:1.

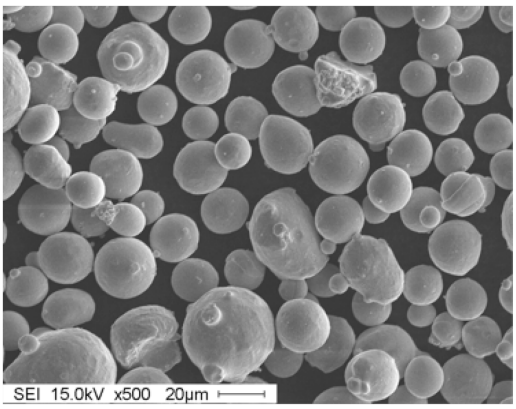

Figure 10: Morphology of the as-received powder

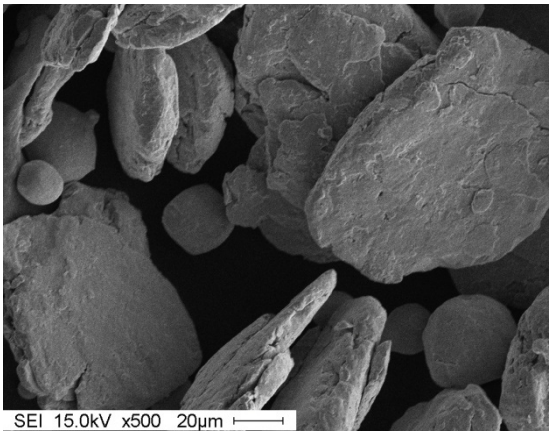

Figure 11: Morphology of the cryomilled CoNiCrAlY feedstock

Table 1: Chemical composition of the Amdry 9951 powder

	Co	Ni	Cr	Al	Y
Composition	38.5	32	21	8	0.5

The cryomilled powder was then HVOF sprayed onto a copper substrate, resulting in a coating of 460 micron in thickness. The copper was then leached in nitric acid to obtain free standing CoNiCrAlY coatings.

The starting and cryomilled powders, and the free-standing coatings were subjected to oxidation. The oxidation experiments, to characterise the surface oxide evolution, were performed in a Linberg Blue furnace. The samples were inserted in the furnace at 1000°C and held at that temperature for duration ranging from 1 to 96 hours. The samples were removed from the furnace, resulting in an air quench. As-sprayed and polished (1200 grit) surfaces were both tested in order to quantify the effect of initial surface condition.

X-ray diffraction (XRD) patterns were obtained with a Philips PW1830 X-Ray Diffractometer. The regular scans were performed between 30° and 80° with a step scan of 0.005° and a time per step of 0.5 seconds. A pure silicon standard (JCPDS # 27-1402) and a time per step of 5 seconds were used for the lattice parameter calculations. Scanning Electron Microscopy (SEM) observations were carried out with a JEOL JSM-840A coupled with EDAX™ EDS and a Hitachi S-3000N VP-SEM with Oxford INCA EDS. Both the surfaces and cross-sections of the powders and coatings were observed for oxide layering and phase distribution, as well as composition. TEM observations were carried out on a Phillips CM200 at an operating voltage of 200 kV. Grain size was measured through image analysis from both bright and dark field images.

2.3 RESULTS

2.3.1 Cryomilling of the CoNiCrAlY feedstock

The selected parameters for the cryomilling of the feedstock were based on the work carried out by Tang et al. on the same material [102] and for which conditions yielded an average grain size of 15nm. The XRD patterns of the starting and milled powders are presented in Figure 12. The peaks of the two main CoNiCrAlY phases are present for the as-received powder, the higher peaks being the γ/γ' phase (JCPDS #15-0806) and the smaller peaks being the β phase (JCPDS #20-0019). Broadening of the peaks is characteristic of an increase of strain in the particles as well as a refinement of the grain size. However, it was observed that peak broadening occurred on the milled powder and that the peak corresponding to the β-phase disappeared, which may be attributed to the dissolution of the β-phase. Phase dissolution resulting from severe plastic deformation, such as in milling processes, has been reported for other systems [142, 143] and thus strengthens the current results. In addition, Richer et al [138] have shown that the stability of the β-phase crystal structure to be lower than the FCC γ phase for the same system. Unfortunately, due to the convolution of the first γ/γ' and β peaks the necessary individual broadening of these two peaks could not be measure, hence grain size measurement via the peak broadening method was not possible.

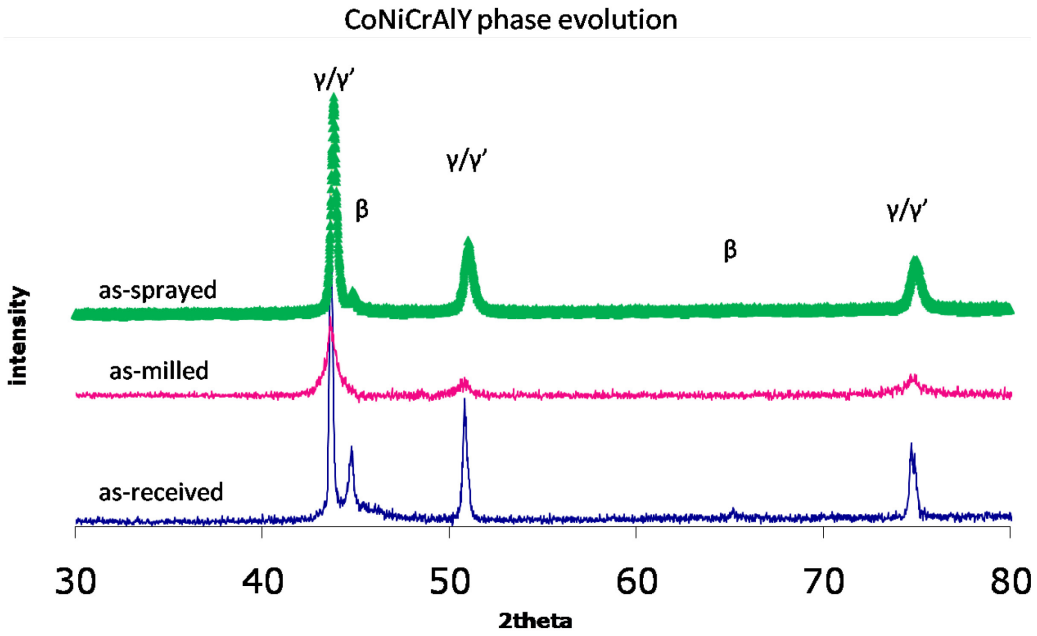

Figure 12: XRD diffraction spectra of original and as-milled powder and as-sprayed coating

2.3.2 Oxidation of CoNiCrAlY feedstock

Figure 13 shows a two-layer oxide scale on the conventional powder after 96h of oxidation at 1000°C. EDS analysis was performed on the scale and the results indicate that the inner layer is composed of Al and O, suggesting Al_2O_3, while the outer layer, which is lighter in color is associated with a mixed oxide as Cr, Ni, Co and O were detected.

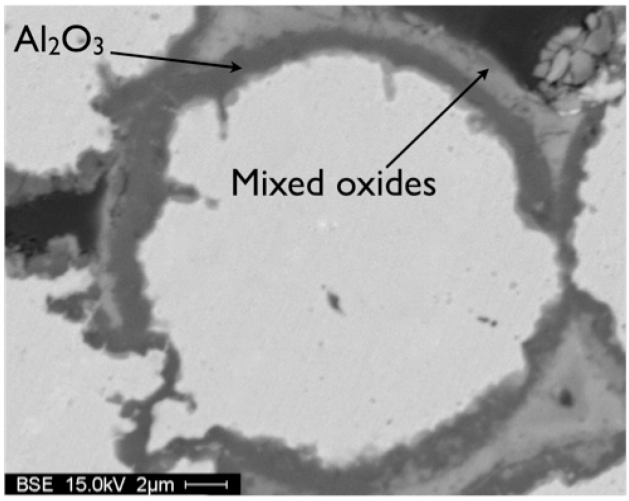

Figure 13: Conventional CoNiCrAlY feedstock particle after 96h of oxidation at 1000°C

For the nanostructured powder, only a single layer of α-Al_2O_3 has been observed on the surface of CoNiCrAlY up to oxidation times of 96h, as depicted in Figure 14.

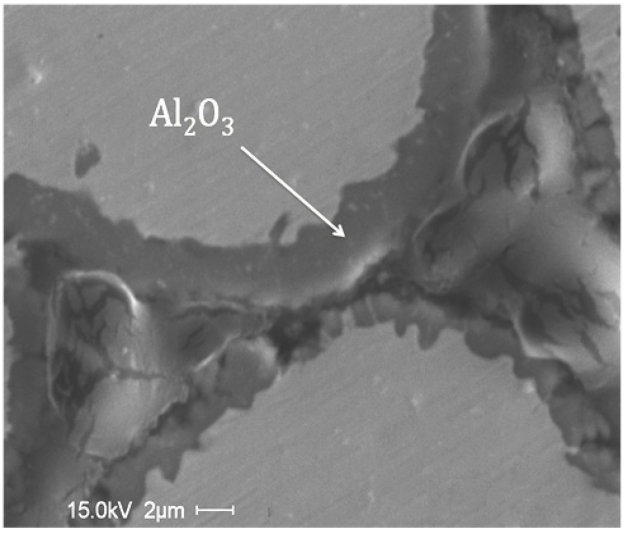

Figure 14: Nanostructured CoNiCrAlY powder after 96h of oxidation at 1000°C

The oxidation of the powders confirms the theory that nanostructuring favors the formation of Al_2O_3 as presented in section 2.1. In fact, the mixed oxide layer that formed on the conventional powder was totally suppressed on the nanostructured powder after oxidation times up to 96h.

2.3.3 Characterization of the nanostructured HVOF coatings

Figure 15 shows an SEM image of the cross-section of a CoNiCrAlY nanostructured coating obtained by HVOF. The coating possesses a low level of porosity. The oblong shape of the particles suggests considerable deformation upon impact during the spraying process, which confirms that the particles did not melt during spraying. Vickers micro-hardness measurements with a load of 100g revealed a value of 371±71.

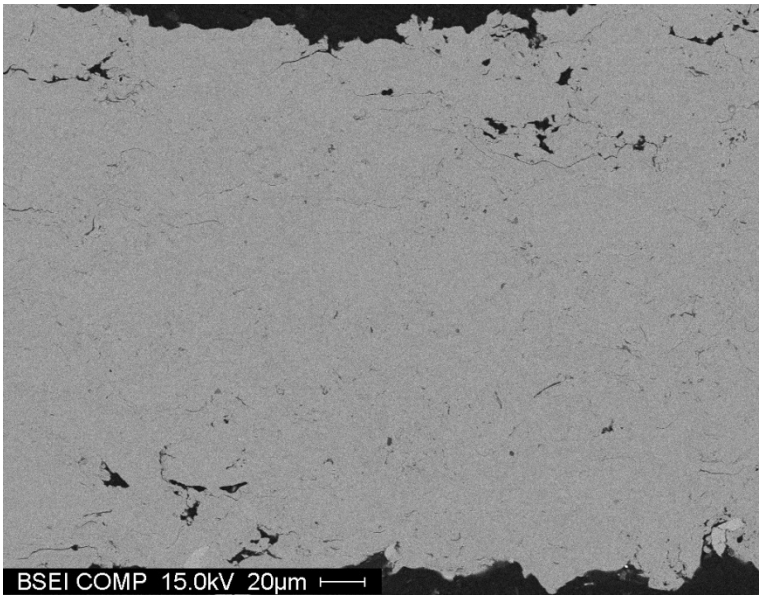

Figure 15: Cross-section of an as-sprayed nanostructured CoNiCrAlY coating

The XRD pattern of the deposited coating is represented as the top line in Figure 12. As can be seen by the reappearance of the first β-phase peak and the sharpening of the γ peaks, the spraying process has induced some phase transformations. This could be attributed to either a release of strain and a growth of the γ and β phases causing a de-convolution of the peaks or to a re-precipitation of the β phase from a supersaturated solid solution caused by the milling.

Figure 16 shows a selected area diffraction (SAD) TEM image. The ring formation is characteristic of a nano-size grain distribution and the presence of few spots indicates the presence of a small number of larger grains. Figure 17 shows a TEM dark field image of the nanostructured CoNiCrAlY coating. Both very small and larger grains can be observed. The grain size distribution, shown in Figure 18, indicates a bimodal distribution where most of the grains are between 20nm and 60nm meaning that the nano grain size was remained after spraying. However, there are some bigger grains around 100nm. Two theories can be proposed to explain the presence of these bigger grains. Either the larger grains grew from existing nano-grains near the surface because of heat input while spraying, or they originate from the core of the particle which was subject to less deformation during milling.

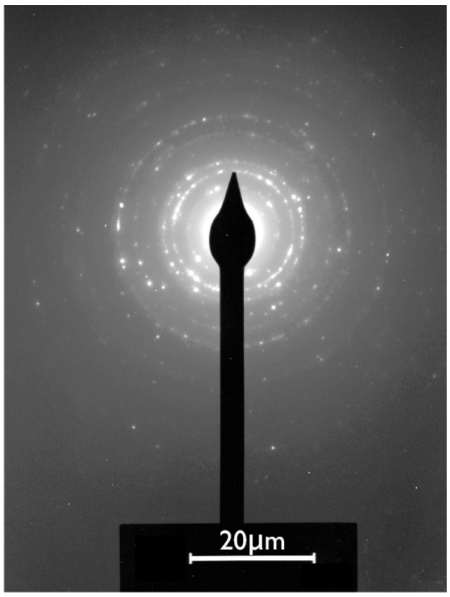

Figure 16: Selected area diffraction (SAD) of an as-sprayed HVOF CoNiCrAlY coating

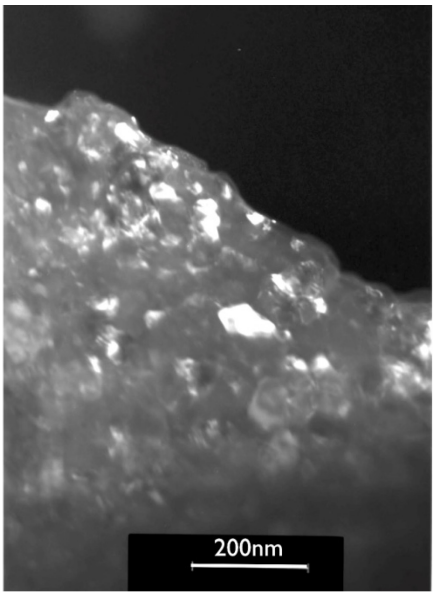

Figure 17: Dark field image of an HVOF as-sprayed CoNiCrAlY coating

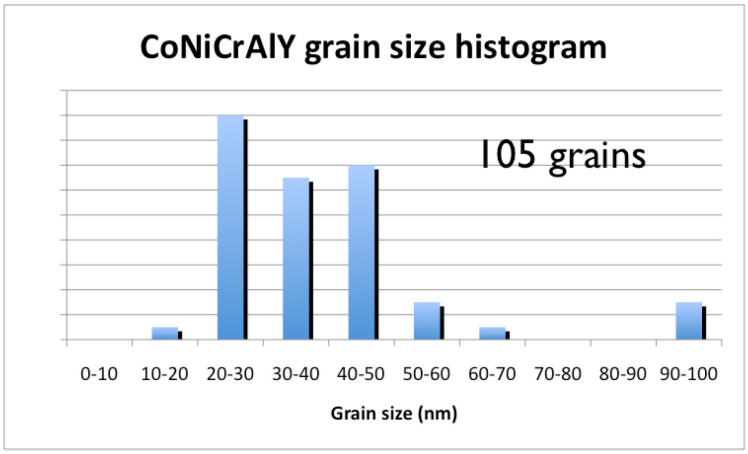

Figure 18: Histogram of the grain size of the CoNiCrAlY as-sprayed coating

2.3.4 Oxidation of as-sprayed nanostructured coatings

Oxidation of the as-sprayed coating has been the subject of some contradiction in the literature. In fact, Tang et al. have reported that a single, pure, oxide scale composed of α-Al_2O_3 and θ-Al_2O_3 grew on top of a nanostructured CoNiCrAlY

coating deposited by HVOF after 24h of oxidation at 1000°C [114]. However, Tang et al. have also reported the formation of a duplex oxide scale composed of an inner layer of α-Al_2O_3 and an outer layer of mixed oxides for the same system and oxidation conditions[102].

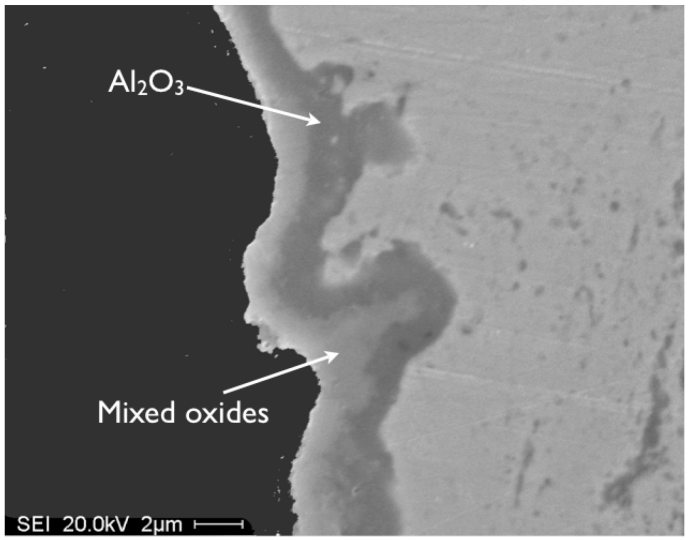

Figure 19: Oxide scale on a CoNiCrAlY coating made from nanostructured powder after 48h of oxidation at 1000°C.

Figure 19 depicts the cross-section of a nanostructured coating oxidized at 1000°C for duration of 48 hours. Figure 20 shows the XRD spectra corresponding to a coating possessing a two-layer oxide, where the innermost layer is α-Al2O3 (JCPDS #48-0366) and the top layer is composed of mixed oxides, mainly $CoAl_2O_4$ (JCPDS #44-0160). Despite the fact that a two-layer scale developed at the surface of the coating, no perpendicular cracks were observed. Such a feature is indicative of a TGO that has a better thermo-mechanical match with the coating and that its adhesion strength is greater, which ultimately yields an improved resistance to spalling.

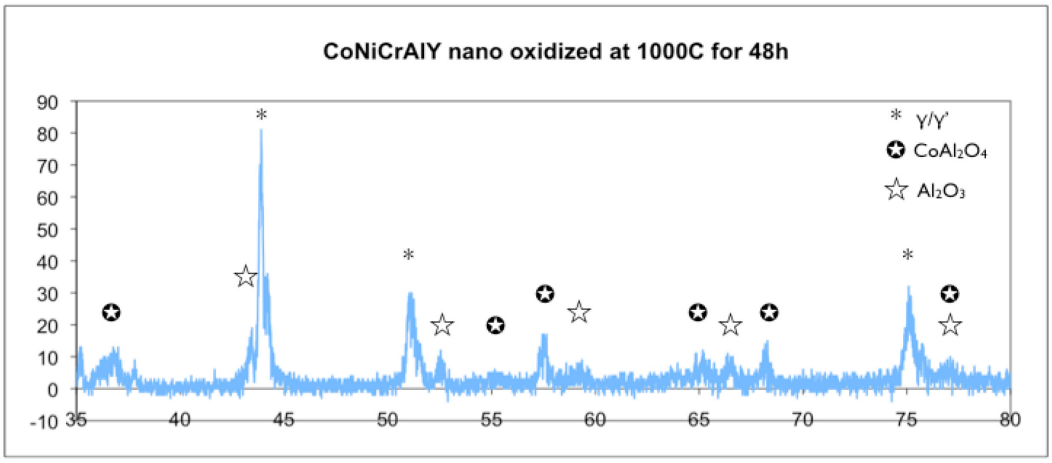

Figure 20: XRD spectrum of a nano un-polished CoNiCrAlY coating after 48h of oxidation at 1000°C.

2.3.5 Oxidation of polished coating surface

Previous work done by Ajdelsztajn et al.[99] mentioned that Al_2O_3 oxide dispersions developed during the cryomilling process are believed to be responsible for the fast

nucleation of α-Al_2O_3. They have based their explanation on the work of Burlin et al.[96] who observed that additives can have an influence on the transformation of metastable alumina to α-Al_2O_3. In particular, they found that small dopant ions, such as Al^{3+}, can accelerate the transformation of the metastable close-packed structure of alumina to the hexagonal close-packed structure of α-Al_2O_3. To verify this hypothesis, the previously oxidized nanostructured coating surfaces were ground down using 1200 grit to remove any surface oxidation and were then subjected to the same oxidation treatment.

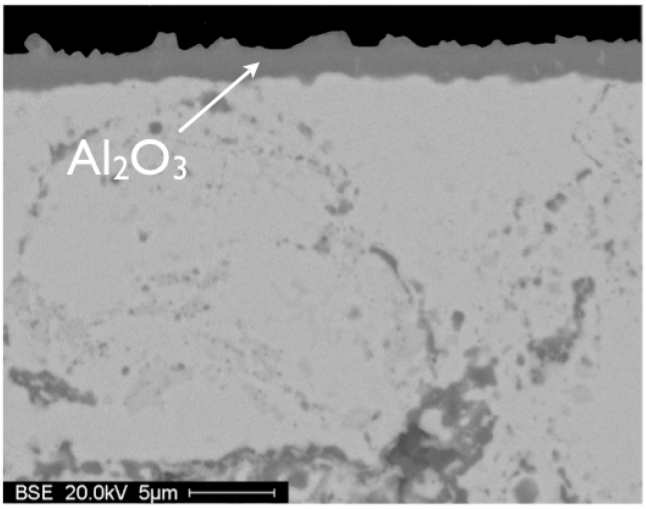

Figure 21: Oxide formation of a polished nanostructured CoNiCrAlY coating after 48h of oxidation showing a single alumina layer.

Figure 21 shows a cross-section of a surface-modified coating exhibiting only a single Al_2O_3 layer, as determined by EDS. These results suggest that the HVOF process is an important variable that might be responsible of the formation of the duplex scale during the static oxidation tests. Moreover, it seems that the effect of the presence of Al_2O_3 dispersoids previously described may have a lower impact on

the seeding of Al_2O_3 as previously suggested by Ajdelsztajn; only the surface treatment was sufficient to yield the desired single scale layer on the same system. It is worth noting that in the case of an oxidized coating from which the scale has been removed, two possible follow-up situations arise. First, if the newly exposed surface in contact with the oxidative environment corresponds with the Al-depleted zone, it is expected that a mixed oxide scale will develop due to insufficient Al present in the coating. In this case the dispersoids would have no scale selectivity effect. Alternatively, if the exposed surface is still rich in Al, the presence of dispersoids may help reformation of the alumina scale. Under these conditions, however, the distribution of Al and grain size of the Beta phase as well as the overall grain size and volume fraction of grain boundaries would all have changed, given the temperature of its initial oxidation. This in turn will affect the diffusion of Al with respect to the as-sprayed coating. Consequently the oxide evolved may or may not yield the desired alumina.

2.4 DISCUSSION

2.4.1 Grain size and in flight oxidation

The oxidation tests done on the powder support the theory that modifying the grain structure of CoNiCrAlY into the nano-regime promotes the selective oxidation of alumina. However, it does not hold true for the as-sprayed nanostructured coatings. As can be seen from Figure 14 and Figure 19, a single layer oxide formed on the

powder but a duplex layer oxide grew on the coating made from the starting feedstock. Two theories have been previously proposed to explain the delay/acceleration in the growth of the second layer. The first one assumes that the surface roughness of the as-sprayed coating is responsible for the growth of the second layer [144]. The second theory proposes that the second layer evolves because of artifacts, such as pre-oxidation sites, formed during spraying [102]. Figure 22 shows a montage of the cross-section of a polished nanostructured coating presenting two different behaviors. The left hand side of the micrograph depicts a ground region where a single alumina scale has developed. The right hand side of the micrograph illustrates a region of the coating unaffected by the grinding operation where the resulting TGO is composed of a two-layer oxide. Since the immediate localized roughness in both regions is the same but the oxide formation differs, the surface roughness is not thought to be a determining factor in oxidation behavior. It is rather thought that small oxide seeds of mixed oxides are formed as a result of the non-equilibrium oxidation during spraying and that grinding the surface removes those seeds, enabling the formation of a single alumina layer.

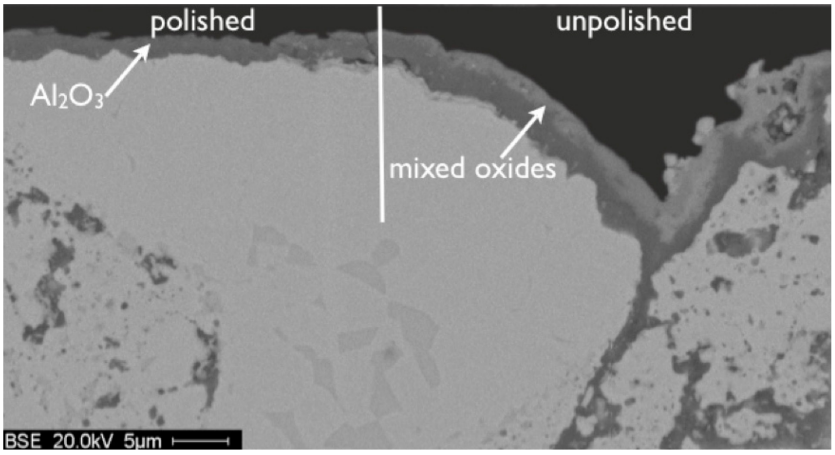

Figure 22: Oxide formation on a polished CoNiCrAlY coating after 48h at 1000°C showing both a single and duplex oxide scale.

2.4.2 Al distribution and TGO

The formation of fast growing oxides such as spinels and Cr_2O_3 is often detrimental to the oxide layer because of the stresses they impose on the scale. Thicker oxide scales should spall from the coating earlier when exposed to thermal cycling. This is due to the elastic strain energy per unit of oxide/metal interface that is stored in the oxide layer upon cooling which increases with increasing oxide thickness [97]. The growth rate of the oxide can be greatly reduced by promoting the formation of a defect free and less permeable Al_2O_3 layer. It is believed that some of the defects present in the TGO are the results of the phase transformation in alumina. The residual stresses associated with the volumetric contraction during the phase transformation of θ-Al_2O_3 to α-Al_2O_3 cause faster diffusion and some cracking of the Al_2O_3 scale, increasing the TGO growth rate. However, Pint et al. have reported that it is possible to avoid this transformation with the presence of alumina dispersoids

in β-NiAl, which yield a direct nucleation of α-Al_2O_3 and an absence of θ-Al_2O_3 [134]. However, as presented previously, there seems to be no need for the alumina dispersoids if the grain structure is in the nano-regime. Therefore, the faster transformation of θ-Al_2O_3 to α-Al_2O_3 observed on the nanostructured CoNiCrAlY coatings is beneficial to oxidation resistance. The formation of a laterally homogeneous and dense α-Al_2O_3 layer that is uniform over the whole surface of the coating will retard the formation or result in a thickness reduction of the mixed oxide layer.

To promote the exclusive formation of α-Al_2O_3, the concentration of aluminum below the oxide/metal interface has to be high enough to ensure its fast diffusion during the early stage of oxidation[145]. Different cases need to be considered. In the case of the oxidation of a single phase system, such as the NiAl intermetallic, the concentration of aluminum is uniform everywhere below the oxide/metal interface which results in a consistent alumina layer. However, the situation is more complex with multi-component systems exhibiting a binary phase microstructure such as MCrAlY (considering only the γ-Ni and the β-NiAl phases). In such a case, both phases need to allow growth of α-Al_2O_3 oxide in order to have an exclusive and laterally homogeneous oxide scale. This is promoted by (1) the formation of a large volume fraction of small β precipitates and (2) increasing the Al content in the γ phase [146, 147]. However, this cannot be achieved under equilibrium conditions as the aluminum content in each phase is fixed by thermodynamics.

Coatings made from cryomilled powders favor the formation of the α-Al_2O_3 oxide layer in two ways when compared to their conventional counterpart. First, during cryomilling the powder is subject to excessive plastic deformation, which may causes the dissolution of the β-phase into the γ-phase as can be observed by the XRD peaks in Figure 3 (see cryomilled spectra). This could imply that the γ phase is enriched with the aluminum that was originally in the β-phase, providing a uniform concentration of aluminum at the surface of the coating. The disappearance of the peak could also imply that the Al originally present in the β-phase could segregate to the grain boundaries. To discriminate between the two situations, the lattice parameters of the gamma and beta phase were measured and the results are presented in Table 2. The starting powder was annealed to 800°C for 1 hour to homogenize the microstructure and the lattice parameter of both phases was compared to reference values. As depicted, the lattice parameter for the γ phase is similar than the literature value, which encompasses the reflections for the γ/γ'. Regarding the β-phase, the lattice parameter is slightly lower than the value reported, corresponding to an intermetallic phase enriched in Ni, but still within the stoichiometric range corresponding to NiAl [148]. The milled powder was heat treated at 900°C, which correspond to a temperature allowing enough distinction of the β-peak for accurate measurements of the lattice parameters. It is important to note that the grain size was still in the nano-regime after heat treatment. When comparing the lattice parameters of the starting and milled/heat treated powders, for both phases, the lattice parameters is lower the than reference value. This would suggest that some of the larger Al atoms, which are present mainly in the β-phase

but also in the γ' phase of the peak identified γ, have moved to the grain boundaries. This segregation will be accompanied by an enrichment in Ni, which would also contribute to a reduction of the lattice parameter. Cryomilled materials are characterized by high-angle grain boundaries, which can easily accommodate larger atoms[57], like Al in the present case. The increased concentration of Al at the grain boundaries would be beneficial for the scale development as grain boundary diffusion is known to be a few order of magnitude higher than lattice diffusion[149]. Secondly, the accompanied increase in grain boundaries due to nanostructuring increases the number of diffusion paths for aluminum towards the surface. In fact, Gao et al. [150] have demonstrated that in the NiCrAlY system, the minimum Al concentration required to form a complete α-Al_2O_3 was reduced by 1/3 for nano-crystalline coatings compared to conventional micron-grain coatings. Therefore, the increase in grain boundaries along with their high concentration of segregated aluminum favor the fast nucleation and growth of Al_2O_3.

Table 2: Lattice parameter comparison for CoNiCrAlY phases

	Lattice parameter (Å)	
sample	Beta phase	Gamma phase
cryomilled annealed at 900°C	2.8639	3.5698±0.0008
original annealed at 800°C	2.8732	3.5799±0.0018
Reference [107]	2.880	3.582

2.4.3 Other means of promoting the formation of a single layer

In the previous sections, it was demonstrated that by changing the microstructure and the aluminum distribution of the feedstock powder the oxidation performance of the resulting coating could be enhanced. However, the results show that a full microstructure modification throughout the coating might not be needed for two reasons. Firstly, the initial stage of oxidation is the most critical and it is surface controlled. Secondly, the nanostructure and desired Al distribution will be lost after only a few hours at 1000°C, which may modify the subsequent oxide development. Therefore, it is possible that a microstructure modification of only the coating surface may yield similarly improved oxidation resistance.

To verify the hypothesis that altered processing parameters might be sufficient, HVOF spraying of the conventional CoNiCrAlY powder with low heat and high velocity were performed and a cross-section of the coating is depicted in Figure 23. The coating is of poor quality and contains numerous unbonded particles. In this case, the sprayed temperature was too low to cause partial melting of the particles and the coating is composed of mechanically interlocked deformed particles. Interestingly, after 48h of oxidation at 1000°C, as opposed to the duplex scale observed on the oxidized feedstock powder (see Figure 4), the oxide scale is dominated by an Al_2O_3 layer with few regions showing a duplex scale, as shown in Figure 24. This change in oxidation behavior could be related to a near-surface modification of the microstructure resulting from the plastic deformation imposed on the particle by the combination of low heat and very high velocity typical of

HVOF. Grain refinement of the surface to the nano-scale is possible; this type of refinement to nano-scale upon particle impact at high velocity was observed in a cold dynamic gas spraying (CDGS) [138]. The particle velocity measured in the CDGS report was 558±95m/s [138], in the same velocity range of a typical HVOF, i.e. ~550m/s. Richer at al. [138] have observed that local but severe plastic deformation imposed at the surface of the particles during CDGS produces significant grain refinement, for which a grain size as small as 20-30 nm was observed by TEM. In addition, the XRD spectrum of the CDGS sprayed CoNiCrAlY coating is characterized by the same grain refinement (broadening) and dissolution of the β-NiAl phases that were observed in the cryomilled powder [138]. These have only been observed on the outer region of the sprayed particle where the strain caused by the deformation is maximized. Despite the desired oxidation behavior, the spraying parameters used to produce the coating presented in Figure 14 would not be used as severe integrity problems of the deposited coating would occur.

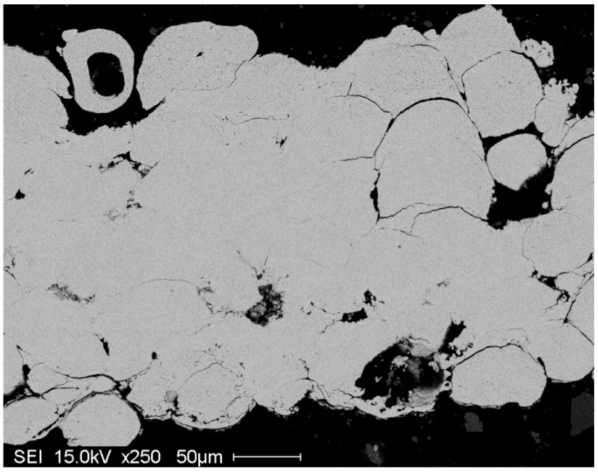

Figure 23: As-sprayed CoNiCrAlY coating from the conventional powder showing a lack of metallurgical bonding.

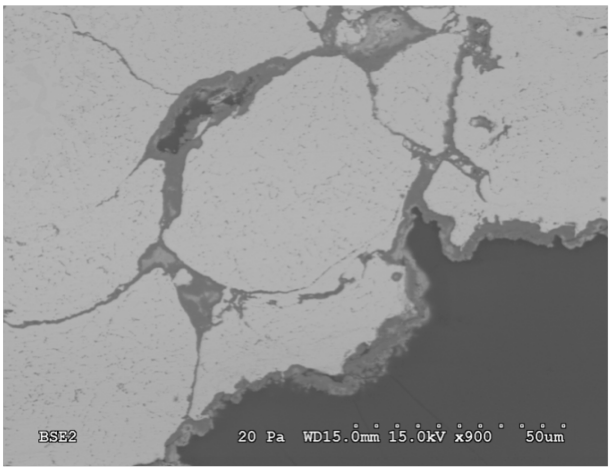

Figure 24: HVOF CoNiCrAlY coating made from conventional powder after 48h of oxidation

2.4.4 Influence of the thermal spray process

In order to substantiate a potential explanation for the oxidation behavior of MCrAlY systems, a literature review of various MCrAlY systems including variables such as spraying process, type of powder feedstock, surface condition prior to oxidation and oxidation conditions is summarised in Table 3.

Only studies in which the oxidation was carried out in the temperature range of 900 to 1100°C were considered, as higher temperature would result in significantly faster oxidation kinetics. Similarly the compiled results contain only short oxidation experiments as it is obvious that once the Al-depleted zone is formed, the Cr-based scale will develop, as this oxide is also thermodynamically possible; this occurs independently of the processing route used. Finally, only work on the oxidation of single coatings was considered as oxidation beneath a top-coat layer should modify the scale-development.

Table 3: Summary of oxidation results for different spraying techniques for MCrAlY systems

System	Conv or Nano	Spraying process	Scale composition	Surface condition before oxidation	Temp and time	Reference
CoNiCrAlY	N (cryomill)	HVOF	Al2O3 and mixed oxide	As sprayed	24h at 1000°C	[102]
CoNiCrAlY	N (cryomill)	HVOF	Al2O3	Ground	24h at 1000°C	[114]
NiCrAlY	N (planetary)	Cold spray	Al2O3	Shot peened	900 and 1000°C for 200 hrs	[137]
NiCrAlY	N (planetary)	Cold spray	Al2O3 and mixed oxide	As sprayed	900 and 1000°C for 200 hrs	[137]
NiCrAlY	N (cryo)	HVOF	Al2O3 and mixed	As sprayed	24 and 95 hours @ 1000°C	[99]
All MCrAlY	C	VPS	Al2O3 and some localized mixed (minor)	As sprayed	1000°C; 1000hrs	[98]
CoNi	C	HVOF	Al2O3 and some mixed	Ground	950°C for various time	[100]
CoNi	C	HVOF	Al2O3	Polished	950°C for various time	[100]
CoNi	C	HVOF	Al2O3	EB-remelted	950°C for various time	[100]
CoNi	C	HVOF	Al2O3 and mixed oxide	As-sprayed	950°C for various time	[100]
CoNi	C	HVOF	Al2O3 and mixed	As-sprayed	950°C for 100 hrs	[151]
CoNi	C	HVOF	Al2O3	EB-remelted	950°C for 100 hrs	[151]
CoNi	C	HVOF	Al2O3 and mixed	As-sprayed	1100°C for 1-100hrs	[64]
CoNi	C	VPS	Al2O3 and mixed	As-sprayed	1100°C for 1-100hrs	[64]
CoNi	C	VPS and HVOF	Al2O3	Heat treated 1100C for 3hr	1100°C for 1-100hrs	[64]
CoNi	C	HFPD	Al2O3 +CoAl2O4	As-sprayed	1000°C for 20 cycles of 8h	[139]
NiCo	C	VPS	Transient Al2O3	Vacuum heat treated and aged	950 and 1050 for 5 to 18 hour	[96]
NiCo	C	HVOF	Only a-Al2O3	Vacuum heat treated and aged	950, 1050 and 1200°C for 25h	[96]
NiCo	C	VPS	Al2O3	2h at 1125 +24h 845	1050°C for 6	[107]
CoNi	C	VPS	Al2O3	2h at 1125 +24h 845	1050°C for 6	[107]
NiCrAlY	C	VPS	Al2O3	As-sprayed	1000°C for 100h	[95]
CoNi	C	VPS	Al2O3+mixed oxides	As-sprayed	1000°C for 1-100h	[119]
NiCrAlY	C	APS	Al2O3 (1000C) Al2O3+mixed (1100)	As-sprayed	1000-1100°C for 50h	[152]

As reported in previous studies [63, 101], it is hypothesized that oxygen pick-up during spraying might be cause for the early formation of a second layer through the formation of oxide seeds at the surface of the coating. Thus, the pre-oxidation (formation of seed) must be considered similar for each layer deposited. Work by Tang [102, 114] shows that for the same material, the removal of the top portion of the coating prevents the formation of the Cr-based scale. This implies that the removal of material exposes fresh coating to the oxidant environment and consequently negates any effect of oxide seeds formed at the surface of the splats. However if oxidation were to be occurring during the coating process, the coating would also contain significant levels of internal oxidation, which is actually a cause for rejection of the coatings. In addition, during the oxidation of a polished surface, the local presence of some mixed-oxide protrusion would be expected as the inter-splat region could contains the seeds, but such feature is not reported in the work describing the formation of a single layer. Therefore, it could be hypothesised that the surface artifacts causing the formation of the second scale could be forming during the cool-down of the coating once the last layer has been deposited, which brings into play the cooling atmosphere. To verify this hypothesis, a comparison of the oxidation behavior of HVOF and VPS was conducted, in which we can assume a lower oxygen pick-up occurred during the cooling of the VPS coatings. Indeed, in as-sprayed conditions, the VPS coatings [95, 98] show mainly Al2O3 scale. In addition, EB-PVD coatings, which are performed under diffusion pump vacuum level (cool down in low oxygen environment), also yield a single Al2O3 scale[90]. On the other hand, most of HVOF coatings [64, 99, 100, 102, 119, 151] exhibit the Cr-based

second scale layer. This comparison seems to reinforce the concept that cooling environment could be the cause for formation of the surface nucleation points causing the development of the second scale. It is worth mentioning that obviously, for uncontrolled processes, this hypothesis is not valid, such as VPS work reported in [119]. The coatings in this study yielded a two-layer scale, but significant oxygen levels at the surface of the coatings upon spraying were reported, which could be the reason for the inability of the VPS process to prevent the formation of the second scale. Changes in surface condition through post-spraying treatment were also found to play an important role in the development of scales in the early stage of oxidation. Two different situations were observed: for as-sprayed or roughly ground surfaces, the coatings exhibited the Cr-based scale [100], while for surface treatments inducing larger modifications, such as EB-remelting or polishing, only the alpha-Al2O3 scale was present[100, 151]. The two latter surface treatments are believed to fully remove the artifacts created during deposition and expose fresh surfaces of metal to the oxidizing environment. Interestingly, another post-spraying operation was found to prevent the formation of the second scale, which is a vacuum heat-treatment. This treatment was found to favour the formation of only the alumina scale during the early oxidation stage regardless of the spraying process used [64, 96, 107]. Based on the Ellingham diagram, the vacuum heat treatment may favour the decomposition of surface oxide precipitates, which would yield a surface free of nucleation points for the formation of the Cr-based scale. Finally, the comparison of the nanostructured powder versus conventional powder is not as straightforward. In all cases, for as-sprayed condition with HVOF [102, 114, 137] the

coatings exhibit two scales, which is in line with the surface oxidation occurring during spraying. One should note that the present work has demonstrated that nanostructuring results in the formation of a single Al2O3 layer on the feedstock and a two-layer scale on the coatings, strengthening the conclusion that the spraying process causes the change in oxidation behavior. It could be hypothesised that a non-thermal process, such as cold spray could be key in preventing the formation of the surface inclusions. To date, only one work was found on cold spray of nanostructured NiCrAlY and the results are showing the formation of two scales in the as-sprayed condition[137]. An important point in this case, however, is that the powders were prepared by planetary milling, a process that would increase the oxygen pick-up during milling when compared to cryomilling. Moreover, the shot-peening treatment was found to prevent the formation of the Cr-based scale, which again, is in line with the removal of the surface inclusions and/or renewal of the exposed surface. Unfortunately, no work on VPS of cryomilled MCrAlY powders has yet to be found in the literature.

2.5 CONCLUSION

A nanostructured coating was obtained by HVOF spraying of a cryomilled CoNiCrAlY feedstock powder. The oxidation experiments conducted at 1000°C for various times on the nanostructured CoNiCrAlY showed that the oxidation behavior is different between the cryomilled powder and the HVOF deposited coating. In particular, the conventional feedstock yielded a duplex oxide scale composed of

Al_2O_3 and mixed oxide, while the nanostructured feedstock grew a single Al_2O_3 layer. However, the nanostructured coatings responded similarly to the conventional powder during the oxidation experiments. It was found that the spaying process considerably modifies the scale evolution, possibly due to oxide seeds formed during the flight of the particles. However, formation of the mixed oxide layer can be avoided through surface polishing prior to oxidation. Also, the milling process has induced phase dissolution of the β-NiAl phase and the lattice parameter measurements indicates that the dissolution should be accompanied with Al-enrichment of the grain boundaries, which contributes to the development of the α-Al_2O_3 scale through faster diffusion of the Al atoms towards the surface.

Chapter 3. *Thermal Stability and Oxidation Behavior of Nanostructured NiCoCrAlY Coatings*

Dominic Mercier[1], Bryan D. Gauntt[2] and Mathieu Brochu[1]

[1]Department of Materials Engineering, McGill University, Montreal, Qc, Ca

[2] Department of Materials Science and Engineering, The Pennsylvania State University, University Park, PA

3.1 INTRODUCTION

A primary challenge of the gas turbines industry is to increase operating temperature as high as possible, the current landmark to surpass being 1000°C. This would result in an efficiency increase as well as a gas emission reduction. However, the harsh environment in the hot end zone limits the type of material used for the combustor, the transition ducts and the turbine blades to nickel superalloys which cannot exceed 600-650°C without losing strength[132], hence the desire to develop new materials that can withstand higher temperatures. To this end, the thermal barrier coating (TBC), which consists of a yttria-partially-stabilized zirconia topcoat and a MCrAlY (M=Ni, CoNi or NiCo) bond coat, has been developed to protect the nickel superalloy components. This, in turn, yields a working temperature around 1000°C. To date, most of the research on NiCoCrAlY has been focused on the TBC

system where it is used as a bond coat. However, the good high temperature oxidation characteristics of the MCrAlY systems allow these alloys to also be used as stand-alone coatings.

The high temperature oxidation resistance of NiCoCrAlY is attributable to its ability to produce a thermally grown oxide (TGO) composed of Al_2O_3 and Cr_2O_3 when exposed to an oxidative environment. Despite many years of research, the service life of a NiCoCrAlY coating is still dependant on the ability of the coating/TGO interface to absorb the thermo-mechanical mismatch between the coating and the oxide layer. Fast growing oxides such as NiO, Cr_2O_3, $CoAl_2O_4$ and $NiAl_2O_4$ impose stresses on the coating/TGO interface, which has been found to cause spallation of the oxide layer[89, 153]. It is therefore crucial to induce the preferential oxidation of Al over Cr to form the more protective and adherent Al_2O_3. The growth rate of stable α-Al_2O_3 (corundum) is slower than that of Cr_2O_3, minimizing thermal stresses. The slower diffusion of cations and oxygen through the α-Al_2O_3 crystal lattice results in a slow growing and dense oxide[115, 135]. However, alumina can initially grow as different metastable structures such as θ-Al_2O_3, γ-Al_2O_3 and δ-Al_2O_3 prior to developing as stable corundum α-Al_2O_3[133]. The different growth mechanisms of the metastable structures and their volumetric changes, which can be as high as 12% for the transformation from θ-Al_2O_3 to α-Al_2O_3, can have considerable influence on the reliability of the TGO[133, 134]. Direct formation of α-Al_2O_3 (or formation at lower temperature) would be preferable.

The integrity of the oxide scale growing on top of NiCoCrAlY is dependent on the nature of the oxide. It has been shown by Lou et al. that the nature of the oxide scale is not only dependent on the chemistry of the alloy but also on the grain size of the coating on which the scale is grown[136]. They demonstrated that a nanostructured K38G superalloy, obtained by sputtering, exhibited oxide selectivity over the as-cast counterpart by forming Al_2O_3 instead of Cr_2O_3 when oxidized at 1000°C. Furthermore, many studies have demonstrated that the oxidation behavior of MCrAlY coatings can be tailored by the use of nanostructured precursors [99, 113, 114, 137]. The selective oxidation of aluminum and the formation of a uniform α-Al_2O_3 scale observed on nanostructured coatings can be attributed to the higher density of nucleation sites and faster solute diffusion, which is provided by the increase in volume fraction of grain boundaries and reduction in lattice diffusion distance[123, 124]. In addition, Wang reports that the high number of grain boundaries per unit area characteristic of nanostructured coatings considerably improves the adherence of the oxide scaledue to pegs formed along the grain boundaries[49].

MCrAlY coatings have been obtained by various techniques such as vacuum plasma spray (VPS)[63, 95, 96, 107, 119], electron beam physical vapor deposition (EB-PVD)[154], air plasma spray (APS) [62, 152, 155], high frequency pulse detonation (HFPD) [139] and high velocity oxygen fuel (HVOF)[62, 63, 96, 99, 100, 102, 103, 114, 141, 156-158]. In recent years, HVOF sprayed coatings has been particularly interesting because they possess high density, strong substrate adhesion and are able to maintain nano-scale structure after spraying [91]. Moreover, HVOF spraying

is performed at atmospheric temperature, resulting in a substantial cost savings compared to the other techniques.

The objective of this study was to investigate the oxidation behavior of nanostructured NiCoCrAlY coatings by means of static oxidation tests in air. Cryomilled powder was subjected to different heat treatments to evaluate its thermal stability. The results were then compared with the oxidation response of nanostructured coatings to try to define the importance of the spraying process. Moreover, an attempt was made at evaluating the influence of the aluminum distribution on the oxidation response of the nanostructured coatings.

3.2 EXPERIMENTAL PROCEDURE

Cryomilling of commercially available gas atomized Ni-171 NiCoCrAlY (-325 mesh) powder was performed using the parameters described by Ajdelsztajn et al. [99] which yielded nanostructured CoNiCrAlY. The original powder morphology is depicted in Figure 25 and the chemistry is presented in Table 1. The milling was performed in a Union Process 1-S attrition mill at 180 RPM for 16h with a ball to powder ratio of 30:1. Liquid nitrogen was constantly added to compensate for evaporation and stearic acid was added as a process control agent at 0.2% by weight, in order to prevent agglomeration of the powder and to facilitate the breakage of the particles.

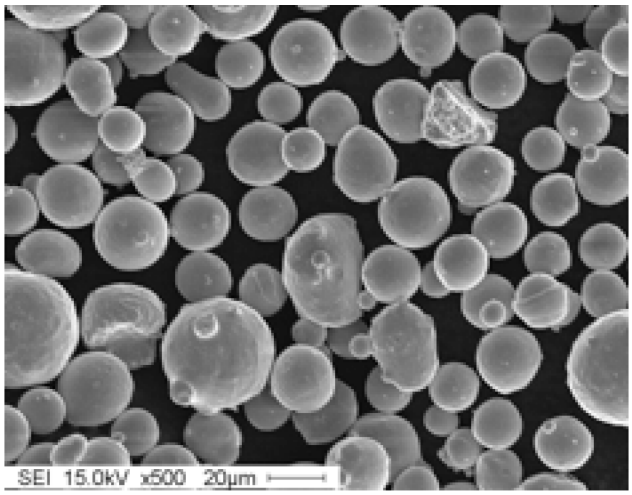

Figure 25: SEM micrograph of the original NiCoCrAlY powder

The cryomilled NiCoCrAlY powder was sprayed by Raymor Industries Inc. in Boisbriand, Qc, Canada, onto a copper substrate using the HVOF process. The copper was subsequently leached out in nitric acid resulting in freestanding coatings slightly thinner than 500 microns.

Table 4: Chemical composition of the Amdry 9951 NiCoCrAlY powder

	Ni	Co	Cr	Al	Y
Composition	46.5	23	17	13	0.5

In order to characterize the oxidation behavior of NiCoCrAlY, the starting and cryomilled powders as well as the freestanding coatings were subjected to oxidation treatments. The samples were inserted in a Linberg Blue furnace at a temperature of 1000°C and held at that temperature for durations ranging from 1 to 96h. The samples were then removed, resulting in an air quench. This oxidation treatment

was done on coatings possessing two different surface finishes, as sprayed and 1200 grit polished.

Annealing treatments followed by oxidation test were also executed on the cryomilled powder in order to quantify the thermal stability of the nanostructured powder and the effect of starting grain size on the oxidation behavior of NiCoCrAlY. The annealing treatments were done for 1 hour in a vacuum furnace at 500, 700 and 900°C. The furnace was equipped with a diffusion pump, the controlled environment was purged twice with argon prior to the test, and titanium sponge was used as a local getter.

Scanning Electron Microscopy (SEM) work was carried out on a JEOL JSM-840A coupled with a EDAX™ EDS and a Hitachi S-3000N VP-SEM with Oxford INCA EDS. The cross-section of the powders and the coatings samples were mounted in a conductive carbon based resin. The x-ray diffraction characterization was performed on a Philips PW1830 X-Ray Diffractometer between 30° and 80° 2θ with a step scan of 0.005 and a time per step of 0.5 seconds. The scans used for lattice parameter calculations followed same parameters but with a time per step of 5 seconds and a pure silicon standard (JCPDS # 27-1402) for peak reference. Transmission electron microscopy (TEM) was performed using a JEOL 2010 with a LaB_6 emitter operated at 200 KeV. A 34μm objective aperture was used for both bright field and dark field images.

3.3 RESULTS

3.3.1 Cryomilling of the NiCoCrAlY feedstock

Figure 26 depicts a series of XRD patterns showing the evolution of the powder during milling and spraying. The bottom line represents the spectra of the original NiCoCrAlY powder, and the two main phases, the γ/γ' (JCPDS #15-0806) phase, a solid solution of Ni, Co and Cr and the β-phase (JCPDS #20-0019), the aluminum rich NiAl, were detected. Figure 27 shows the cross-section of an as-received NiCoCrAlY particle. The lighter phase corresponds to the γ/γ' phase and the darker phase is the β-phase.

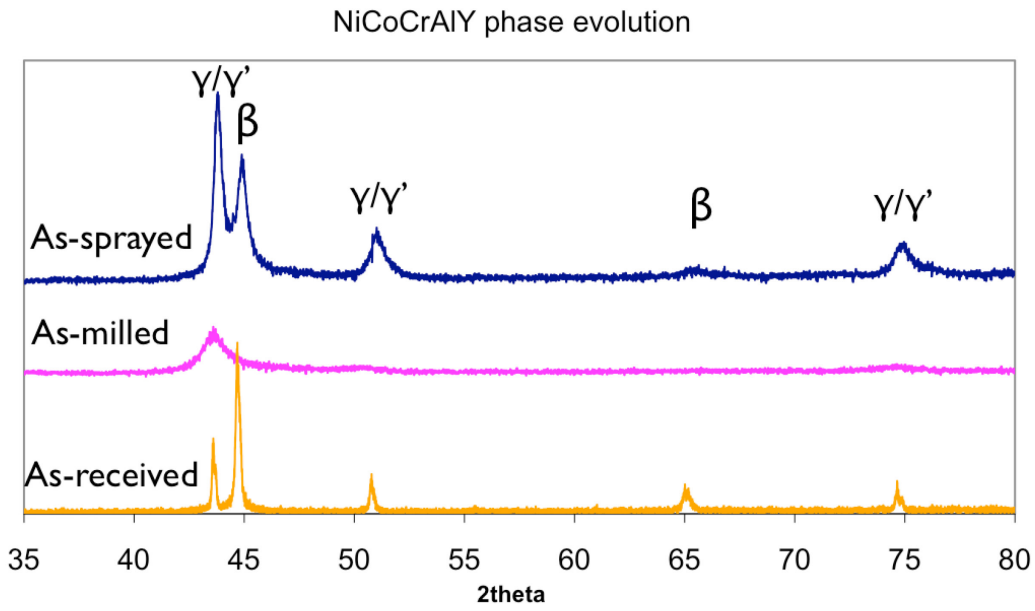

Figure 26: Phase evolution of NiCoCrAlY

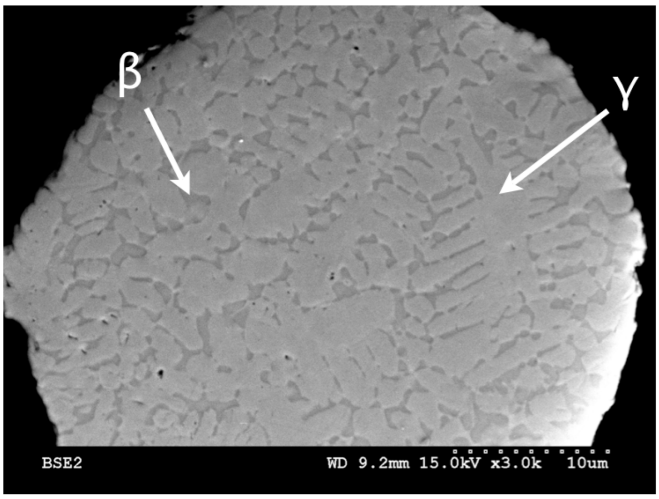

Figure 27: Cross-section of the original particle showing the two main phases, Beta and Gamma

The morphology of the cryomilled NiCoCrAlY particles after 8 and 16 hours can be seen in Figure 28 and Figure 29 respectively. The rough oval shape of the powder after 8h of milling is characteristic of high levels of deformation having not yet resulted in a full nanostructure. However, the flakiness of the particles after 16h of milling suggests that the grain size is in the nano-regime. In fact, Tang et al. obtained an average grain size of 15nm with the same cryomilling parameters for a CoNiCrAlY alloy[114]. The XRD pattern of the milled powder is shown as the middle spectrum in Figure 26. Considerable broadening and reduction of intensity of the γ/γ' peak can be observed. These are characteristics of a reduction in grain size as well as an increased lattice strain. In addition, the absence of the β peak on the milled powder spectrum can be attributed to the dissolution of the β-phase during milling. Phase dissolution resulting from severe plastic deformation, as in milling processes, has been previously reported by Horita et al. [33] and Bakker[142, 143]. Moreover, it has been shown by Richer et al. that the stability of the β-phase BCC

crystal structure is lower than that of the FCC γ-phase for the similar CoNiCrAlY system [138], reinforcing the current findings. Unfortunately, it is impossible to measure the grain size of the milled powder through the peak broadening technique due to the convolution of the γ/γ' and the β peaks.

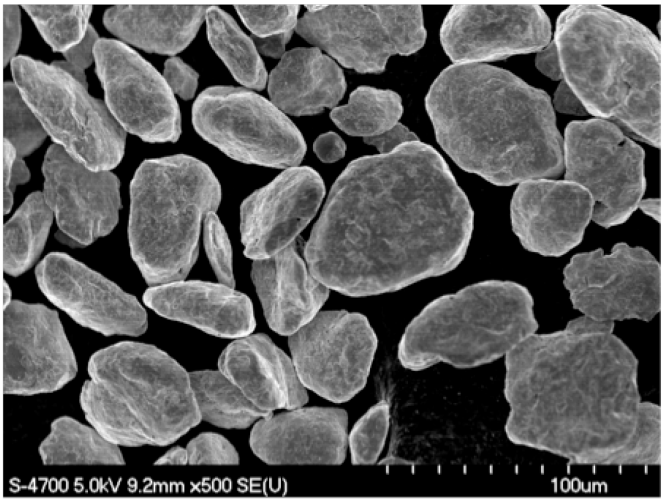

Figure 28: SEM micrograph showing the morphology of the NiCoCrAlY particles after 8h of cryomilling

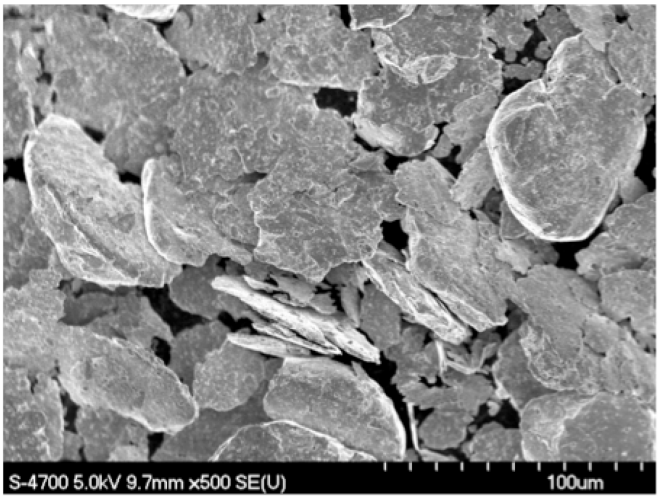

Figure 29: SEM micrograph showing the morphology of the NiCoCrAlY particles after 16h of cryomilling

3.3.2 Characterization of the nanostructured HVOF coating

A secondary electron micrograph of the cross-section of the NiCoCrAlY coating obtained by the HVOF spraying technique is presented in Figure 30. The volume fraction of porosity is quite low. Vickers micro-hardness measurements with a load of 100g revealed an average value of 434±64 HV which is similar to the value of 438 HV300 reported by Itoh et al. [159].

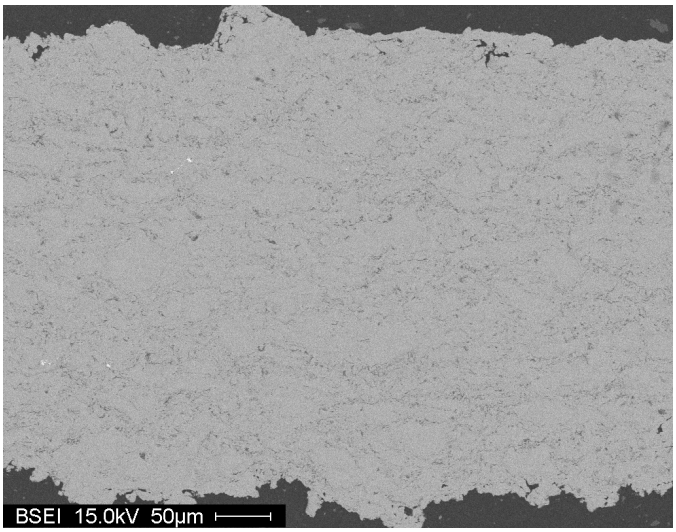

Figure 30: Cross-section of the as-sprayed NiCoCrAlY coating obtained by HVOF

The upper line in Figure 26 shows the XRD pattern of the as-sprayed NiCoCrAlY coating made from cryomilled feedstock. Considerable growth and sharpening of the γ/γ' peaks and a reappearance of the β peak can be noted. Changes in the XRD patterns can be caused by a release of strain in the particles which induces a growth of the γ/γ' and β peaks leading to a deconvolution of said peaks. They can also be

caused by a re-precipitation of the β-phase from the supersaturated solid solution matrix. Interestingly, the peak intensity for the β-phase phase on the starting powder is preeminent, while for the nanostructured coatings γ/γ' is the primary phase, indicating that the thermal spray process induces partial phase recovery in the coating.

TEM observations through the selected area diffraction (SAD) pattern and the dark field image shown in Figure 31 revealed that the crystal structure of the as-sprayed coating remained in the nano-regime even after thermal exposure during the spraying. Broad diffraction ring formation in the SAD pattern is characteristic of a nano-size grain distribution. Also, it is assumed that both phases underwent grain refinement down to the nano-regime because their corresponding rings are both complete and relatively thick. Nano-grain size can be further confirmed by the TEM dark field micrograph. The average grain size measured was 10.5±5.5 nm.

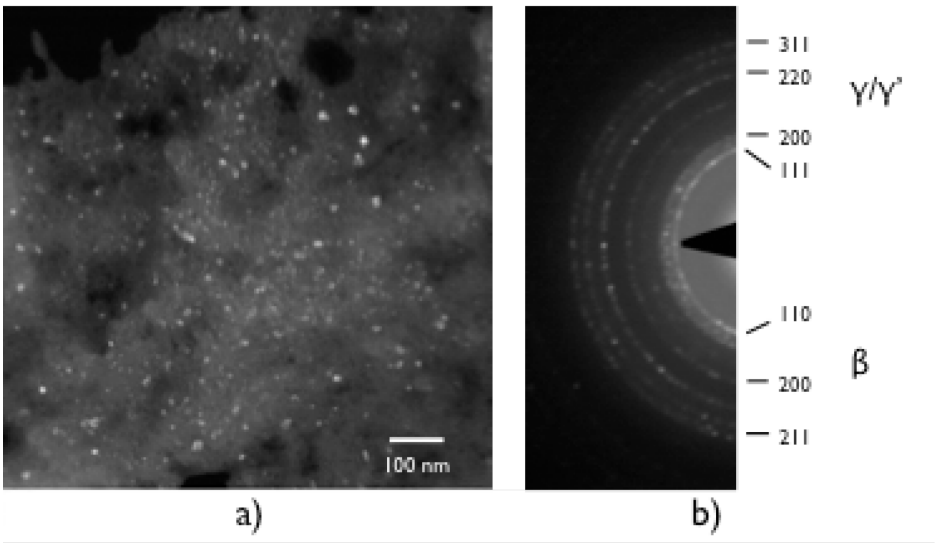

Figure 31: a) Dark Field micrograph of the nanostructured NiCoCrAlY coating deposited by HVOFand b) corresponding selected area diffraction

3.3.3 Thermal stability of nanostructured NiCoCrAlY powders

Thermal stability of the nanostructured powders has been evaluated through different heat treatments. Figure 32 shows a collection of XRD spectra of the two main peaks of the NiCoCrAlY powder heat treated at 500, 700 and 900°C, respectively. It is important to note that only the first two peaks had high enough intensity for evaluation. It can be observed that the cryomilled powder exhibits good thermal stability at temperatures below 500°C as no significant peak deconvolution was observed. Growth of the γ/γ' and β peaks begins at 700°C. However, the SAD pattern and bright field image of the powder heat-treated at 700°C, presented in Figure 33, clearly show that the grain size is still in the nano-regime. Scherer's equation was used to calculate grain size,

$$B(2\theta) = {0.9\lambda}/{D\cos(\theta)}$$

where D is the crystallite size, B(2θ) is the peak broadening at half maximum intensity in radians, λ is the wavelength of the x-ray radiation and θ is the Bragg angle. Previous work on nanostructured systems has shown that nearly complete stress relaxation from milled powder occurred at annealing temperature above 0.3 T_m[160]. It can therefore be assumed that in the present case, peak broadening is caused solely by the refinement in grain size since the annealing temperatures are above $0.3T_m$, and the calculation for the sample heat treated at 700°C yielded a grain size of 63nm.

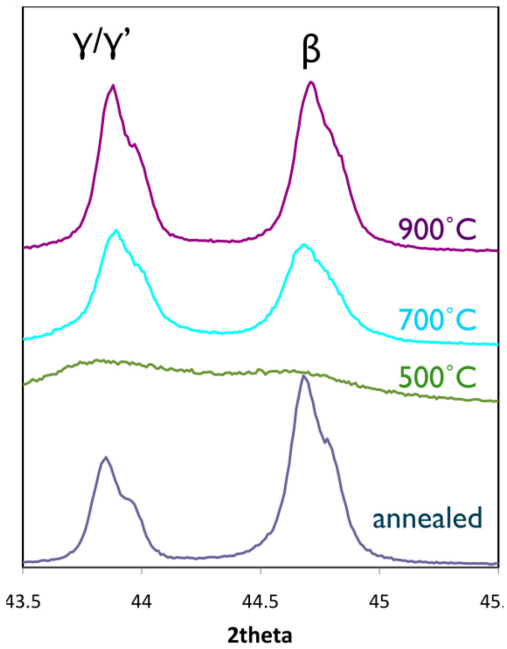

Figure 32: XRD spectra showing phase evolution of the NiCoCrAlY powder after heat treatments of 1 hour at various temperatures

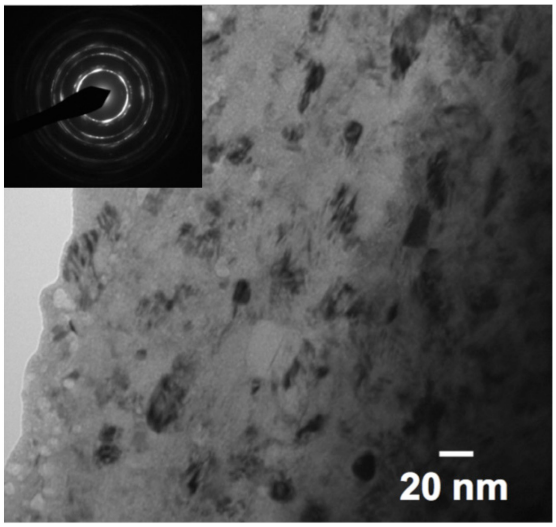

Figure 33: TEM bright field image and SADP of a heat-treated NiCoCrAlY powder at 700C for 1h in vacuum

Using the same procedure, the grain size of the heat-treated powder at 900°C was calculated to be 251nm; the larger grains in the TEM bright field image, and the loss of complete rings in the SAD, as shown in Figure 34, agree with the calculations.

These results show that the thermal stability of nanostructured NiCoCrAlY powders is better than nanostructured Inconel 625 at 700°C [130] but is lower than similar nanostructured Inconel 718 which exhibited grain size stability up to 800°C [161]. Through a comparison of the ratio of intensity for the γ/γ' and the β reflections of the heat treated powders (see Figure 32) with the nanostructured coating (see Figure 26), it can be hypothesised that the spraying process induced a lower thermal load than a heat treatment for 1 hour at 700°C. This also supports the TEM grain size measurement results as the coatings maintained a smaller grain size.

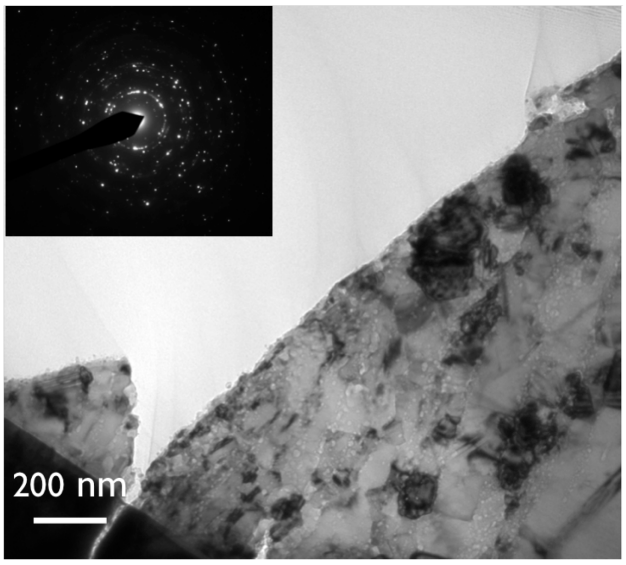

Figure 34: TEM bright field and SADP of the cryomilled NiCoCrAlY powder heat-treated in vacuum at 900C for 1h

3.3.4 Oxidation of nanostructured coatings

The oxidation of HVOF sprayed nanostructured NiCoCrAlY coatings has not been extensively studied compared to the NiCrAlY and CoNiCrAlY systems. Figure 35 is a

backscattered image showing the cross-section of the as-sprayed nanostructured coating oxidized for 48h at 1000°C. The TGO is composed of two oxide layers. Through the combination of the EDS and XRD analysis shown in Figure 36, the composition of the upper layer has been identified as Cr, Ni, Co, Al and O suggesting the fast growing spinels $NiAl_2O_4$ (JCPDS# 20-0781) and $CoAl_2O_4$ (JCPDS# 44-0160). The inner layer is α-Al_2O_3 (JCPDS# 48-0366). No delamination and no perpendicular cracks are observed within the TGO and at the TGO/coating interface. This is due to an improved thermo-mechanical matchup of the oxide with the coating and should result in an improved resistance to spalling.

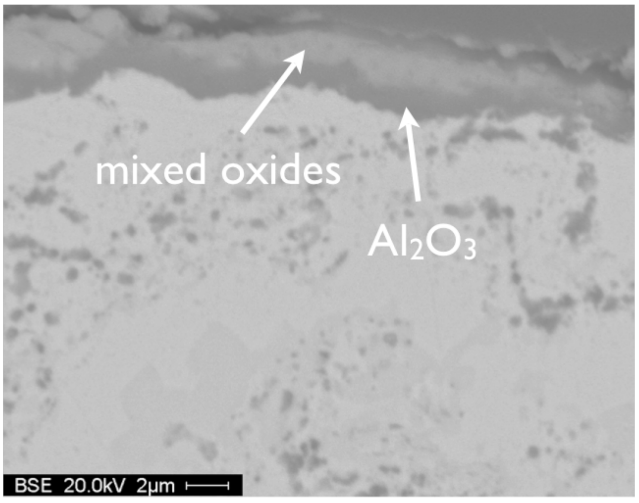

Figure 35: Back-scattering electron micrograph of a nanostructured NiCoCrAlY coating after oxidation for 48 hrs at 1000°C

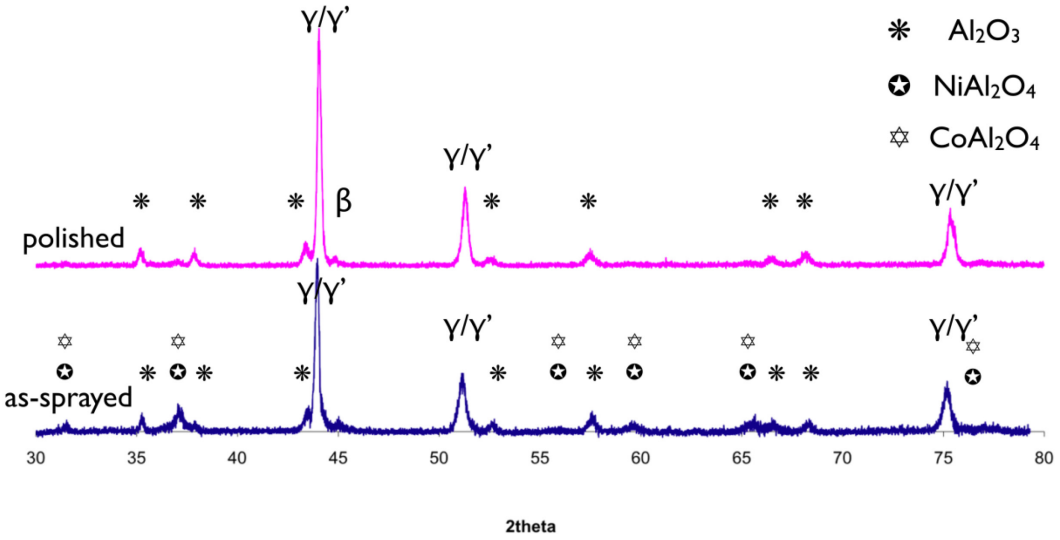

Figure 36: XRD patterns of the TGO on thenanostructured NiCoCrAlY coating oxidized for 48 hrs at 1000°C in both the as-sprayed and polished surface condition.

To study the effect of surface state on oxidation, the surface of the coating was ground with 1200 grit sandpaper prior to an oxidation treatment at 1000°C for 48h. A backscattered micrograph of the TGO is presented in Figure 37. As depicted, the scale is composed of solely a single and well bonded layer of α-Al_2O_3. This was confirmed by XRD analysis in Figure 36. As shown in the upper spectra, no undesired spinels have formed after 48h oxidation heat treatment on the polished coating.

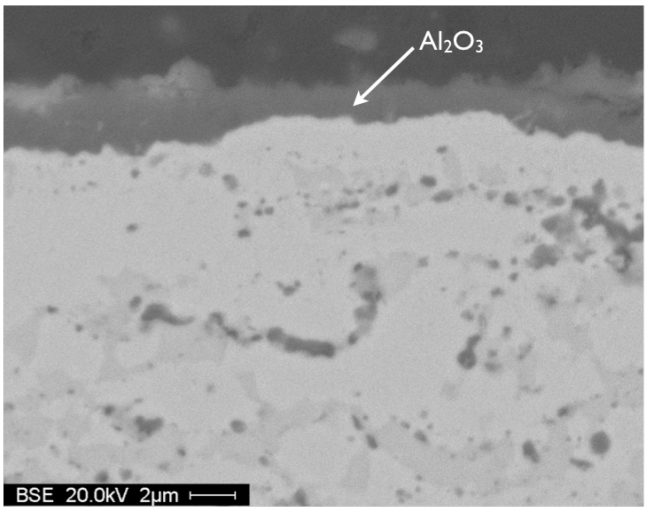

Figure 37: Back scattering electron micrograph of the polished top surface of nanostructured NiCoCrAlY coating oxidized for 48h at 1000C

3.4 DISCUSSION

3.4.1 Influence of the aluminum distribution and nanostructure of the oxidation behavior

To maximize the performance of a MCrAlY coating, it is important to develop strategies to promote the early formation of a laterally homogenous and slow growing oxide that does not allow for fast diffusion of undesirable ions. In addition, this oxide scale has to be well bonded with the coating and needs to be able to absorb thermo-mechanical stresses over a large range of temperature. Thus, fast growing oxides such as Cr_2O_3, $NiAl_2O_4$ and $CoAl_2O_4$ are detrimental to the long-term quality of the oxide scale because of the stresses they impose on the TGO during thermal cycling. Spallation of thick oxide layers occurs earlier when compared to thinner layers because of the elastic strain per unit area of oxide/metal interface

stored in the oxide layer[97]. Hence, the growth rate of the oxide layer can be reduced by the formation of Al_2O_3[156]. It is worth mentioning that the volumetric change associated with the phase transformation from θ-Al_2O_3 to α-Al_2O_3 causes considerable internal stress and cracking, which was found to increase the growth of the oxide layer through diffusion in high strain regions and defects. Therefore, the rapid and early transformation from θ-Al_2O_3 to α-Al_2O_3 observed on nanostructured NiCoCrAlY provides a denser alumina layer, which should decrease the growth rate of the TGO.

The formation of an exclusive α-Al_2O_3 layer depends strongly on the microstructure of the deposited coating. In multi-component systems showing a binary phase distribution such as in NiCoCrAlY, the oxidation behavior is dependent on the size and the form of the second phase[146]. It has been shown that the two primary phases in MCrAlY systems, γ and β, can form alumina scales but their oxidation behavior is different. In fact, transient metastable aluminum oxides have been reported to nucleate first on the β-phase whereas the slow growing α-Al_2O_3 initially form on the γ-phase[162]. To avoid the formation of residual stresses caused by the phase transformation of alumina, microstructural changes are needed to promote an exclusive and laterally homogenous oxide scale. Such changes as small β precipitates, a high Al content in the γ phase and a narrow spaced lamellar β-γ structure can promote the early formation of α-Al_2O_3[146, 147, 163].

As observed from the XRD spectra of the nanostructured powder in Figure 26, cryomilling of the powder caused dissolution of the β-phase peak. A complete dissolution of the β-phase would signify that in the early stage of oxidation only γ-phase is exposed on the surface, leading to the nucleation of solely α-Al_2O_3, assuming the initial oxidation occurs prior to the reprecipitation and growth of the beta phase. Severe plastic deformation may have enriched the γ phase with Al contained in the β-phase providing a uniform aluminum concentration leading to homogenous growth kinetics. However, the dissolution of the β-phase could also imply that some of the aluminum content segregated to grain boundaries. Lattice parameter calculations of the gamma and beta phase were performed in order differentiate between the two situations. The calculation results are presented in Table 5. It is important to note that the lattice parameter calculations of the γ phase are based on the positions of the γ/γ' peaks. The cryomilled powder was annealed at 500, 700 and 900°C, which allowed a distinct separation of the γ/γ' and β peaks, enabling accurate determination of their position and made possible the evaluation of the thermal stability of the two phases. For both annealed samples, the lattice parameters of the gamma and beta phases are smaller than the original values. This would suggest that the larger aluminum atoms present mainly in the β-NiAl, but also in the γ'-Ni_3Al, were forced to move to the grain boundaries during milling, causing a Ni enrichment in the γ phase. The enrichment of nickel, having a smaller atomic radius than Al, would be accompanied by a reduction in the lattice parameter. This increase in Al at the grain boundaries can be accommodated by the high-angle grain boundaries characteristic of cryomilled powders. Comparing the lattice parameter

values of the annealed NiCoCrAlY samples to those of CoNiCrAlY [164], it can be concluded that the thermal stability of CoNiCrAlY is better than that of NiCoCrAlY. Consequently, with the higher number of grain boundaries in nanostructured materials, which can reduce the aluminum concentration required to form a continuous α-Al_2O_3 scale by 1/3 compared to conventional material[150], and the fact that grain boundary diffusion is considerably faster than lattice diffusion[149], an increase in aluminum concentration at grain boundaries would have a very positive effect on the alumina scale growth.

Table 5: Lattice parameters of Gamma and Beta phases for different NiCoCrAlY powder conditions studied in this work

	Lattice Parameter (Å)	
SAMPLE	Gamma	Beta
Original annealed at 800°C	3.5762+/- 0.0008	2.8676+/- 0.0003
Cryomilled annealed at 900°C	3.5732+/- 0.0002	2.8657+/- 0.0008
Cryomilled annealed at 700°C	3.5707+/- 0.0006	2.8654+/- 0.0011

3.4.2 Influence of the HVOF process on the oxidation behavior

The different oxidation behavior of the coating in the as-sprayed condition and surface polished condition is significant. Polishing the surface of the coatings resulted in growth of only a single oxide layer. Although no detrimental effect of the second oxide layer on the quality of the coating/oxide system can be observed after 48h, the higher thermo-mechanical stress load imposed by a thick and fast growing

oxide on the whole TGO can have harmful implications at longer oxidation times. Different explanations are proposed for the growth of the second oxide layer on thermally sprayed coatings. It is proposed by Czech et al. [144] that the early formation of the mixed oxide layer is attributed to the surface roughness of as-sprayed coatings. Another explanation, proposed by Tang et al., attributes the rapid nucleation of the mixed oxide layer to artifacts formed during spraying [102]. It was found in this research that the short exposure of the particles to the high temperature during thermal spraying causes a non-equilibrium oxidation of the surface creating small mixed oxide seeds. Hence, polishing the surface removes those seeds. Seed removal, combined with the advantages provided by nanostructure previously detailed, allows for the thermodynamically more stable α-Al_2O_3 to form.

3.5 CONCLUSION

Nanostructured coatings made from cryomilled NiCoCrAlY feedstock were obtained via HVOF. Annealing heat treatments performed for 1h at 700°C on the cryomilled powder revealed a grain size of 63nm, which indicates good thermal stability of the coating. Oxidation experiments conducted on the coating at 1000°C for various times show that a sound and adherent duplex oxide scale develops on the surface. This scale is composed of an inner layer of Al_2O_3 and an outer layer of mixed, fast growing oxides such as Cr_2O_3, $NiAl_2O_4$ and $CoAl_2O_4$. It was shown that the segregation of aluminum and microstructural changes caused by the milling affected

the oxidation behavior by promoting an early nucleation of α-Al_2O_3. Also, it was determined that the spraying process itself was responsible for early formation of the mixed oxide layer due to oxide seeds formed during exposure of the particles to high temperature during spraying.

Chapter 4. *Summary*

The preceding chapters have shown that using nanostructured CoNiCrAlY and NiCoCrAlY powders as feedstock to produce stand-alone coatings by the HVOF spraying technique considerably improves the high temperature oxidation resistance. In Chapter 2, it was shown nanostructured cryomilled CoNiCrAlY powders formed a single Al_2O_3 layer upon high temperature oxidation whereas a duplex oxide layer consisting of an inner Al_2O_3 layer and an upper mixed layer grew on the conventional counterpart. It was demonstrated that the dissolution of the β-NiAl phase during cryomilling creates an enrichment of aluminum at the grain boundaries, which is responsible to the growth of a stable α-Al_2O_3 layer in the early stage of oxidation, thus preventing the formation of mixed oxides. Moreover, the mixed oxide layer found on the coatings was attributed to the nature of the spraying process. Despite the formation of mixed oxides upon high temperature oxidation, which was prevented by grinding the coating's surface after spraying, it is envisioned that nanostructrured CoNiCrAlY coatings can be used as stand-alone coating in harsh oxidizing environments.

The oxidation of nanostructured NiCoCrAlY coatings confirmed the results obtained previously with CoNiCrAlY. It was found that an adherent and defect free oxide scale grew on the NiCoCrAlY coating. In addition, it was shown that the nanostructured NiCoCrAlY powders have good thermal stability comparable to

those of Inconel 625 and 718 produced using the same milling procedure and that nanostructured NiCoCrAlY can also be utilized as oxidation resistant stand-alone coatings.

Future work on the oxidation behavior of nanostructured CoNiCrAlY and NiCoCrAlY project consists in performing experiments in a different oxidative environment more representative of that found in the industrial process. The oxidation behavior of the coatings in an environment richer in sulfur would likely be different. Moreover, a better understanding of the stages leading to alumina phase transformation should be sought. With such knowledge, specific heat treatments favoring the formation of α-Al_2O_3 could be performed prior to long-term oxidation.

Chapter 5. References

1. Zhu, Y., *Nanostructured materials: From laboratory to commercialization.* JOM Journal of the Minerals, Metals and Materials Society, 2006. **58**(4): p. 27-27.
2. Valiev, R.Z., R.K. Islamgaliev, and I.V. Alexandrov, *Bulk nanostructured materials from severe plastic deformation.* Progress in Materials Science, 2000. **45**(2): p. 103-189.
3. Yurkov, G., et al., *Electrical and magnetic properties of nanomaterials containing iron or cobalt nanoparticles.* Inorganic Materials, 2007. **43**(8): p. 834-844.
4. Bonetti, E., L. Pasquini, and E. Sampaolesi, *The influence of grain size on the mechanical properties of nanocrystalline aluminium.* Nanostructured Materials, 1997. **9**(1-8): p. 611-614.
5. Champion, Y., et al., *Near-Perfect Elastoplasticity in Pure Nanocrystalline Copper.* Science, 2003. **300**(5617): p. 310-311.
6. Conrad, H. and K. Jung, *Effect of grain size from millimeters to nanometers on the flow stress and deformation kinetics of Ag.* Materials Science and Engineering A, 2005. **391**(1-2): p. 272-284.
7. Fougere, G.E., J.R. Weertman, and R.W. Siegel, *On the hardening and softening of nanocrystalline materials.* Nanostructured Materials, 1993. **3**(1-6): p. 379-384.
8. Koch, C.C., et al., *Ductility of nanostructured materials.* MRS Bulletin, 1999. **24**(2): p. 54-57.
9. Lu, L., et al., *High-tensile ductility in nanocrystalline copper.* Journal of Materials Research, Febuary 2000. **15**(2).
10. Ovid'ko, I.A. and A.G. Sheinerman, *Enhanced ductility of nanomaterials through optimization of grain boundary sliding and diffusion processes.* Acta Materialia, 2009. **57**(7): p. 2217-2228.
11. Pozdnyakov, V., *Ductility of nanocrystalline materials with a bimodal grain structure.* Technical Physics Letters, 2007. **33**(12): p. 1004-1006.
12. Sanders, P.G., J.A. Eastman, and J.R. Weertman, *Elastic and tensile behavior of nanocrystalline copper and palladium.* Acta Materialia, 1997. **45**(10): p. 4019-4025.
13. Tellkamp, V., E. Lavernia, and A. Melmed, *Mechanical behavior and microstructure of a thermally stable bulk nanostructured Al alloy.* Metallurgical and Materials Transactions A, 2001. **32**(9): p. 2335-2343.
14. Wang, N., et al., *Effect of grain size on mechanical properties of nanocrystalline materials.* Acta Metallurgica et Materialia, 1995. **43**(2): p. 519-528.
15. Wang, Y., et al., *High tensile ductility in a nanostructured metal.* Nature, 2002. **419**(6910): p. 912.
16. Wang, Y.M., et al., *Microsample tensile testing of nanocrystalline copper.* Scripta Materialia, 2003. **48**(12): p. 1581-1586.

17. Weertman, J.R., *Hall-Petch strengthening in nanocrystalline metals.* Materials Science and Engineering: A, 1993. **166**(1-2): p. 161-167.
18. Li, J. and J.Z. Zhang, *Optical properties and applications of hybrid semiconductor nanomaterials.* Coordination Chemistry Reviews. **In Press, Corrected Proof**.
19. Nechaev, Y.S. and O.K. Alexeeva, *On the nature, capability and reversibility of hydrogen storage in novel carbon nanomaterials for mobile power units.* International Journal of Hydrogen Energy, 2003. **28**(12): p. 1433-1443.
20. Savage, T. and A. Rao, *Thermal Properties of Nanomaterials and Nanocomposites*, in *Thermal Conductivity*. 2004. p. 261-284.
21. Gajbhiye, M.B., et al., *Fungus mediated synthesis of silver nanoparticles and its activity against pathogenic fungi in combination with Fluconazole.* Nanomedicine: Nanotechnology, Biology and Medicine. **In Press, Accepted Manuscript**.
22. Gutkin, M.Y., K.N. Mikaelyan, and I.A. Ovid'ko, *Athermal grain growth through cooperative migration of grain boundaries in deformed nanomaterials.* Scripta Materialia, 2008. **58**(10): p. 850-853.
23. Karakasidis, T.E. and C.A. Charitidis, *Vacancy effect on the elastic constants of layer-structured nanomaterials.* Theoretical and Applied Fracture Mechanics, 2009. **51**(3): p. 195-201.
24. Bachurin, D.V., et al., *Diffusion-accomodated rigid-body translations along grain boundaries in nanostructured materials.* Materials Science and Engineering A, 2003. **359**(1-2): p. 247-252.
25. Cao, G., *Nanostructures and Nanomaterials - Synthesis, Properties and Applications*, ed. I.C. Press. 2004: World Scientific. 451.
26. Siegel, R.W., *Cluster-assembled nanophase materials.* Annual Review of Materials Science, 1991. **21**(1): p. 559-578.
27. Dong, X.L., C.J. Choi, and B.K. Kim, *Chemical synthesis of Co nanoparticles by chemical vapor condensation.* Scripta Materialia, 2002. **47**(12): p. 857-861.
28. Chang, W., et al., *Nanostructured ceramics synthesized by chemical vapor condensation.* Nanostructured Materials, 1995. **6**(1-4): p. 321-324.
29. Cushing, B.L., V.L. Kolesnichenko, and C.J. O'Connor, *Recent Advances in the Liquid-Phase Syntheses of Inorganic Nanoparticles.* Chemical Reviews, 2004. **104**(9): p. 3893-3946.
30. Hench, L.L. and J.K. West, *The sol-gel process.* Chemical Reviews, 2002. **90**(1): p. 33-72.
31. Champion, Y. and J. Bigot, *Characterization of nanocrystalline copper powders prepared by melting in a cryogenic liquid.* Materials Science and Engineering A, 1996. **217-218**: p. 58-63.
32. Seto, T., et al., *Synthesis of size-selected silicon nanoparticles by laser ablation.* Journal of Aerosol Science, 2000. **31**(Supplement 1): p. 628-629.
33. Zhang, J. and C.Q. Lan, *Nickel and cobalt nanoparticles produced by laser ablation of solids in organic solution.* Materials Letters, 2008. **62**(10-11): p. 1521-1524.

34. Pingali, K.C., S. Deng, and D.A. Rockstraw, *Direct synthesis of Ru-Ni core-and-shell nanoparticles by spray-pyrolysis: Effects of temperature and precursor constituent ratio.* Powder Technology, 2008. **183**(2): p. 282-289.
35. Jang, H.D., et al., *Synthesis of SiO2 nanoparticles from sprayed droplets of tetraethylorthosilicate by the flame spray pyrolysis.* Current Applied Physics, 2006. **6**(Supplement 1): p. e110-e113.
36. Husseini, G.A. and W.G. Pitt, *Micelles and nanoparticles for ultrasonic drug and gene delivery.* Advanced Drug Delivery Reviews, 2008. **60**(10): p. 1137-1152.
37. Blasi, P., et al., *Solid lipid nanoparticles for targeted brain drug delivery.* Advanced Drug Delivery Reviews, 2007. **59**(6): p. 454-477.
38. Huh, Y., et al., *Control of carbon nanotube growth using cobalt nanoparticles as catalyst.* Applied Surface Science, 2005. **249**(1-4): p. 145-150.
39. Gwinn, M.R. and V. Vallyathan, *Nanoparticles: Health Effects - Pros and Cons.* Environmental Health Perspectives, December 2006. **114**(12).
40. Birringer, R., et al., *Diffusion and Low Temperature Deformation by Diffusional Creep of Nanocrystalline Materials.* Defect and Diffusion Forum. **Diffusion Processes in High Technology Materials**: p. 17-32.
41. Horv·th, J., R. Birringer, and H. Gleiter, *Diffusion in nanocrystalline material.* Solid State Communications, 1987. **62**(5): p. 319-322.
42. Kommel, L., I. Hussainova, and O. Volobueva, *Microstructure and properties development of copper during severe plastic deformation.* Materials & Design, 2007. **28**(7): p. 2121-2128.
43. Chokshi, A.H., et al., *On the validity of the hall-petch relationship in nanocrystalline materials.* Scripta Metallurgica, 1989. **23**(10): p. 1679-1683.
44. Hall, E.O., *The Deformation and Ageing of Mild Steel: III Discussion of Results.* Proceedings of the Physical Society. Section B, 1951. **64**(9): p. 747-753.
45. Schuh, C.A., T.G. Nieh, and T. Yamasaki, *Hall-Petch breakdown manifested in abrasive wear resistance of nanocrystalline nickel.* Scripta Materialia, 2002. **46**(10): p. 735-740.
46. Nieh, T.G. and J. Wadsworth, *Hall-petch relation in nanocrystalline solids.* Scripta Metallurgica et Materialia, 1991. **25**(4): p. 955-958.
47. E. O. Hall, *Yield Point Phenomena in Metals and Alloys*. Plenum Press. 1970, New York.
48. Valiev, R., *Nanostructuring of metals by severe plastic deformation for advanced properties.* Nat Mater, 2004. **3**(8): p. 511-516.
49. Wang, F., *The effect of nanocrystallization on the selective oxidation and adhesion of Al2O3 scales.* Oxidation of Metals, 1997. **48**(3): p. 215-224.
50. Zhang, L., et al., *Shear punch testing and fracture toughness of bulk nanostructured silver.* Materials & Design, 2009. **30**(5): p. 1445-1450.
51. Zhang, L., et al., *Fabrication of bulk nanostructured silver material from nanopowders using shockwave consolidation technique.* Materials Science and Engineering: A, 2008. **487**(1-2): p. 219-227.
52. Ye, J. and J.M. Schoenung, *Technical Cost Modeling for the Mechanical Milling at Cryogenic Temperature (Cryomilling).* Advanced Engineering Materials, 2004. **6**(8): p. 656-664.

53. Suryanarayana, C., *Nanocrystalline materials.* International Materials Reviews, 1995. **40**(2): p. 41-64.
54. Lu, L. and M.O. Lai, *Formation of new materials in the solid state by mechanical alloying.* Materials & Design, 1995. **16**(1): p. 33-39.
55. Rawers, J. and R. Doan, *Mechanical processing of iron powders in reactive and nonreactive gas atmospheres.* Metallurgical and Materials Transactions A, 1994. **25**(2): p. 381-388.
56. Jang, J.S.C., et al., *Microstructure evolution of mechanical alloyed Ni—24 at% Si.* Journal of Materials Science, 1998. **33**(1): p. 265-270.
57. Witkin, D.B. and E.J. Lavernia, *Synthesis and mechanical behavior of nanostructured materials via cryomilling.* Progress in Materials Science, 2006. **51**(1): p. 1-60.
58. Xun, Y., F. Mohamed, and E. Lavernia, *Synthesis of nanocrystalline Zn-22 Pct Al using cryomilling.* Metallurgical and Materials Transactions A, 2004. **35**(2): p. 573-581.
59. Fecht, H.J., *Nanostructure formation by mechanical attrition.* Nanostructured Materials, 1995. **6**(1-4): p. 33-42.
60. Zhang, X., et al., *Evidence for the formation mechanism of nanoscale microstructures in cryomilled Zn powder.* Acta Materialia, 2001. **49**(8): p. 1319-1326.
61. He, J. and J.M. Schoenung, *Nanostructured coatings.* Materials Science and Engineering A, 2002. **336**: p. 274-319.
62. Chen, W.R., et al., *TGO growth behaviour in TBCs with APS and HVOF bond coats.* Surface and Coatings Technology, 2008. **202**(12): p. 2677-2683.
63. Lugscheider, E., C. Herbst, and L. Zhao, *Parameter studies on high-velocity oxy-fuel spraying of MCrAlY coatings.* Surface and Coatings Technology, 1998. **108-109**(1-3): p. 16-23.
64. Saeidi, S., K. Voisey, and D. McCartney, *The Effect of Heat Treatment on the Oxidation Behavior of HVOF and VPS CoNiCrAlY Coatings.* Journal of Thermal Spray Technology, 2009. **18**(2): p. 209-216.
65. Lau, M.L., et al., *Synthesis of nanocrystalline M50 steel powders by cryomilling.* Nanostructured Materials, 1996. **7**(8): p. 847-856.
66. Luton, M.J., et al., *Multicomponent Ultrafine Microstructures.* Materials Research Society Symposium Proceedings, 1989. **132**: p. 79

.
67. Liu, F. and R. Kirchheim, *Nano-scale grain growth inhibited by reducing grain boundary energy through solute segregation.* Journal of Crystal Growth, 2004. **264**(1-3): p. 385-391.
68. Liu, F., et al., *Nano-scale grain growth kinetics.* Thermochimica Acta, 2006. **443**(2): p. 212-216.
69. Bose, S., *High temperature coatings*, ed. BH. 2007, Amsterdam ; Boston Elsevier Butterworth-Heinemann. 299.
70. Cantor, B., P. Grant, and H. Assender, *Aerospace materials*. Series in materials science and engineering, ed. I.o. physics. 2001, Philadelphia: CRC Press. 312.
71. Sivakumar, R. and B.L. Mordike, *High temperature coatings for gas turbine blades: A review.* Surface and Coatings Technology, 1989. **37**(2): p. 139-160.

72. Meetham, G.W., *Requirements for and factors affecting high temperature capability.* Materials & Design, 1988. **9**(5): p. 244-252.
73. Nicholls, J.R., *Advances in coating design for high-performance gas turbines.* MRS bulletin, 2003: p. 659-670.
74. Taylor, T.A. and P.N. Walsh, *Thermal expansion of MCrAlY alloys.* Surface and Coatings Technology, 2004. **177-178**: p. 24-31.
75. Birks, N., G.H. Meier, and F.S. Pettit, *Introduction to the High-Temperature Oxidation of Metals*. Vol. Second Edition. 2006, Cambridge: Cambridge University Press.
76. Nicoll, A.R. and G. Wahl, *The effect of alloying additions on M---Cr---Al---Y systems--An experimental study.* Thin Solid Films, 1982. **95**(1): p. 21-34.
77. Khanna, A.S., *Introduction to High Temperature Oxidation and Corrosion*. 2002, Materials Park: ASM International. 324.
78. Radcliff, A.S., *FACTORS INFLUENCING GAS TURBINE USE AND PERFORMANCE.* Materials Science and Technology, 1986. **3**(7): p. 554-561.
79. Goward, G.W., *Progress in coatings for gas turbine airfoils.* Surface and Coatings Technology, 1998. **108-109**(1-3): p. 73-79.
80. Haynes, J.A., et al., *High-temperature diffusion barriers for protective coatings.* Surface and Coatings Technology. **188-189**: p. 153-157.
81. Tawancy, H.M., et al., *Thermal stability of a platinum aluminide coating on nickel-based superalloys.* Journal of Materials Science, 1992. **27**(23): p. 6463-6474.
82. Warnes, B.M., *Improved aluminide/MCrAlX coating systems for super alloys using CVD low activity aluminizing.* Surface and Coatings Technology, 2003. **163-164**: p. 106-111.
83. Göbel, M., A. Rahmel, and M. Schütze, *The isothermal-oxidation behavior of several nickel-base single-crystal superalloys with and without coatings.* Oxidation of Metals, 1993. **39**(3): p. 231-261.
84. Sun, J.H., H.C. Jang, and E. Chang, *Effects of pretreatments on structure and oxidation behaviour of d.c.-sputtered platinum aluminide coatings.* Surface and Coatings Technology, 1994. **64**(3): p. 195-203.
85. Dust, M., et al., *Structure and 700 [degree]C hot corrosion behavior of chromium modified platinum--aluminide coatings.* Journal of Vacuum Science & Technology A: Vacuum, Surfaces, and Films, 1986. **4**(6): p. 2571-2576.
86. Malush, R.E., P. Deb, and D.H. Boone, *Structure and 900 ∞C hot corrosion behavior of chromium-modified platinum aluminide coatings.* Surface and Coatings Technology, 1988. **36**(1-2): p. 13-26.
87. Goward, G.W. and D.H. Boone, *Mechanisms of formation of diffusion aluminide coatings on nickel-base superalloys.* Oxidation of Metals, 1971. **3**(5): p. 475-495.
88. Sauders, S.R.J. and J.R. Nicholls, *Coatings and surface treatments for high temperature oxidation resistance.* Materials Science and Technology, 1989. **5(8)**: p. 780.
89. Hesnawi, A., et al., *Isothermal oxidation behaviour of EB-PVD MCrAlY bond coat.* Vacuum, 2007. **81**(8): p. 947-952.

90. Li, M.H., et al., *Phase transformation and bond coat oxidation behavior of EB-PVD thermal barrier coating.* Surface and Coatings Technology, 2004. **176**(2): p. 209-214.
91. Strauss, D., et al., *Oxide scale growth on MCrAlY bond coatings after pulsed electron beam treatment and deposition of EBPVD-TBC.* Surface and Coatings Technology, 2001. **135**(2-3): p. 196-201.
92. Brandl, W., et al., *Effects of specimen treatment and surface preparation on the isothermal oxidation behaviour of the HVOF-sprayed MCrAlY coatings.* Surface and Coatings Technology. **188-189**: p. 20-26.
93. Guo, M.H., et al., *Oxidation and hot corrosion behavior of gradient NiCoCrAlYSiB coatings deposited by a combination of arc ion plating and magnetron sputtering techniques.* Corrosion Science, 2006. **48**(9): p. 2750-2764.
94. Vetter, J., et al., *MCrAlY coatings deposited by cathodic vacuum arc evaporation.* Surface and Coatings Technology, 1994. **68-69**: p. 27-31.
95. Seo, D., et al., *High-temperature Oxidation Behavior and Surface Roughness Evolution of VPS NiCrAlY Coating.* Journal of Thermal Spray Technology, 2008. **17**(1): p. 136-143.
96. Toma, D., W. Brandl, and U. Kˆster, *Studies on the transient stage of oxidation of VPS and HVOF sprayed MCrAlY coatings.* Surface and Coatings Technology, 1999. **120-121**: p. 8-15.
97. Evans, H.E., *Stress effects in high temperature oxidation of metals.* International Materials Reviews, 1995. **40**(1): p. 1-40.
98. Seo, D., et al., *Comparative study on oxidation behavior of selected MCrAlY coatings by elemental concentration profile analysis.* Applied Surface Science, 2008. **255**(5, Part 2): p. 2581-2590.
99. Ajdelsztajn, L., et al., *Oxidation behavior of HVOF sprayed nanocrystalline NiCrAlY powder.* Materials Science and Engineering A, 2002. **338**(1-2): p. 33-43.
100. Brandl, W., et al., *Effects of specimen treatment and surface preparation on the isothermal oxidation behaviour of the HVOF-sprayed MCrAlY coatings.* Surface and Coatings Technology, 2004. **188-189**: p. 20-26.
101. Brandl, W., D. Toma, and H.J. Grabke, *The characteristics of alumina scales formed on HVOF-sprayed MCrAlY coatings.* Surface and Coatings Technology, 1998. **108-109**(1-3): p. 10-15.
102. Tang, F., et al., *Effects of surface oxidation during HVOF processing on the primary stage oxidation of a CoNiCrAlY coating.* Surface and Coatings Technology, 2004. **185**(2-3): p. 228-233.
103. Toma, D., et al., *The Characteristics of Alumina Scales Formed on HVOF-Sprayed MCrAlY Coatings.* Oxidation of Metals, 2000. **53**: p. 125-137.
104. Fairbanks, J.W. and R.J. Hecht, *The durability and performance of coatings in gas turbine and diesel engines.* Materials Science and Engineering, 1987. **88**: p. 321-330.
105. Czech, N., F. Schmitz, and W. Stamm, *Improvement of MCrAlY coatings by addition of rhenium.* Surface and Coatings Technology, 1994. **68-69**: p. 17-21.

106. Chaki, T.K., A.K. Singh, and K. Sadananda, *Effects of CoCrAlY coating on microstructural stability and creep behavior of a nickel-base superalloy.* Thin Solid Films, 1989. **168**(2): p. 207-220.
107. Brandl, W., et al., *The oxidation behaviour of sprayed MCrAlY coatings.* Surface and Coatings Technology, 1996. **86-87**(Part 1): p. 41-47.
108. Smeggil, J.G., *Some comments on the role of yttrium in protective oxide scale adherence.* Materials Science and Engineering, 1987. **87**: p. 261-265.
109. Baufeld, B., et al., *Microstructural changes as postmortem temperature indicator in Ni-Co-Cr-Al-Y oxidation protection coatings.* Materials Science and Engineering A, 2004. **384**(1-2): p. 162-171.
110. Mendis, B.G., et al., *Microstructural observations of as-prepared and thermal cycled NiCoCrAlY bond coats.* Surface and Coatings Technology, 2006. **201**(7): p. 3918-3925.
111. Achar, D.R.G., et al., *Modelling of phase equilibria in MCrAlY coating systems.* Surface and Coatings Technology, 2004. **187**(2-3): p. 272-283.
112. Wu, Y.N., et al., *Oxidation behavior of laser remelted plasma sprayed NiCrAlY and NiCrAlY-Al2O3 coatings.* Surface and Coatings Technology, 2001. **138**(1): p. 56-60.
113. Liu, Z., et al., *Oxidation behaviour of sputter-depositedNi-Cr-Al micro-crystalline coatings.* Acta Materialia, 1998. **46**(5): p. 1691-1700.
114. Tang, F., L. Ajdelsztajn, and J.M. Schoenung, *Influence of Cryomilling on the Morphology and Composition of the Oxide Scales Formed on HVOF CoNiCrAlY Coatings.* Oxidation of Metals, 2004. **61**(3): p. 219-238.
115. Brumm, M.W. and H.J. Grabke, *The oxidation behaviour of NiAl-I. Phase transformations in the alumina scale during oxidation of NiAl and NiAl-Cr alloys.* Corrosion Science, 1992. **33**(11): p. 1677-1690.
116. Pettit, F.S., Trans. Metall. Soc. AIME, 1967. **239**: p. 1296.
117. Nijdam, T.J. and W.G. Sloof, *Modelling of composition and phase changes in multiphase alloys due to growth of an oxide layer.* Acta Materialia, 2008. **56**(18): p. 4972-4983.
118. Okamoto, H., *Al-Ni (aluminum-nickel).* Journal of Phase Equilibria and Diffusion, 2004. **25**(4): p. 394-394.
119. Seo, D., et al., *Influence of heat exposure time on isothermal degradation of plasma sprayed CoNiCrAlY coatings.* Surface and Coatings Technology, 2007. **201**(18): p. 7952-7960.
120. Ali, M.S., S. Song, and P. Xiao, *Degradation of thermal barrier coatings due to thermal cycling up to 1150°C.* Journal of Materials Science, 2002. **37**(10): p. 2097-2102.
121. Armijo, J.S., *The kinetics and mechanism of solid-state spinel formation — A review and critique.* Oxidation of Metals, 1969. **1**(2): p. 171-198.
122. Schumann, E. and M. R¸hle, *Microstructural observations on the oxidation of [gamma]'-Ni3Al at high oxygen partial pressure.* Acta Metallurgica et Materialia, 1994. **42**(4): p. 1481-1487.
123. Giggins, C.S. and F.S. Pettit, Trans. TMS-AIME, 1969. **245**: p. 2495.

124. Wang, N., et al., *Room temperature creep behavior of nanocrystalline nickel produced by an electrodeposition technique.* Materials Science and Engineering A, 1997. **237**(2): p. 150-158.
125. Zhong, Y., et al., *Determination of grain size by XRD profile analysis and TEM counting in nano-structured Cu.* Journal of Alloys and Compounds, 2009. **476**(1-2): p. 113-117.
126. Williams, D.B. and C.B. Carter, *Transmission Electron Microscopy: A Textbook for Materials Science*. 1996: Springer.
127. Milligan, J., R. Vintila, and M. Brochu, *Nanocrystalline eutectic Al-Si alloy produced by cryomilling.* Materials Science and Engineering: A, 2009. **508**(1-2): p. 43-49.
128. Suryanarayana, C. and H.G. Norton, *X-ray Diffraction: A Practical Approach*. 1998, New York: Plenum Press.
129. Klug, H.P. and L.E. Alexander, *X-ray diffraction procedures for polycrystalline and amorphous materials*. 1954, New York: Wiley.
130. Chung, K., et al., *Grain growth behavior of cryomilled INCONEL 625 powder during isothermal heat treatment.* Metallurgical and Materials Transactions A, 2002. **33**(1): p. 125-134.
131. Varin, R.A., J. Bystrzycki, and A. Calka, *Effect of annealing on the microstructure, ordering and microhardness of ball milled cubic (L12) titanium trialuminide intermetallic powder.* Intermetallics, 1999. **7**(7): p. 785-796.
132. B. Cantor, P.G., Hazel Assender, *Aerospace materials*. Series in materials science and engineering, ed. I.o. physics. 2001, Philadelphia: CRC Press. 312.
133. Wefers, K. and C. Misra, *Oxides and Hydroxides of Aluminum.* Alcoa Technical paper, 1987. **19**(Alcoa Laboratories).
134. Pint, B., M. Treska, and L. Hobbs, *The effect of various oxide dispersions on the phase composition and morphology of Al2O3 scales grown on β-NiAl.* Oxidation of Metals, 1997. **47**(1): p. 1-20.
135. Evans, A.G., et al., *Mechanisms controlling the durability of thermal barrier coatings.* Progress in Materials Science, 2001. **46**(5): p. 505-553.
136. Lou, H., et al., *Oxide formation of K38G superalloy and its sputtered micrograined coating.* Surface and Coatings Technology, 1994. **63**(1-2): p. 105-114.
137. Zhang, Q., et al., *Study of oxidation behavior of nanostructured NiCrAlY bond coatings deposited by cold spraying.* Surface and Coatings Technology, 2008. **202**(14): p. 3378-3384.
138. Richer, P., et al., *CoNiCrAlY microstructural changes induced during Cold Gas Dynamic Spraying.* Surface and Coatings Technology, 2008. **203**(3-4): p. 364-371.
139. Belzunce, F.J., V. Higuera, and S. Poveda, *High temperature oxidation of HFPD thermal-sprayed MCrAlY coatings.* Materials Science and Engineering A, 2001. **297**(1-2): p. 162-167.
140. Haynes, J.A., et al., *Mechanical properties and fracture behavior of interfacial alumina scales on plasma-sprayed thermal barrier coatings.* Materials at High Temperatures, 1999. **16**: p. 49-69.

141. Wielage, B., et al., *Development and trends in HVOF spraying technology.* Surface and Coatings Technology, 2006. **201**(5): p. 2032-2037.
142. Horita, Z., et al., *Development of fine grained structures using severe plastic deformation.* Materials Science and Technology, 2000. **16**: p. 1239-1245.
143. Bakker, H., G.F. Zhou, and H. Yang, *Mechanically driven disorder and phase transformations in alloys.* Progress in Materials Science, 1995. **39**(3): p. 159-241.
144. Czech, N., et al., *Influence of the surface roughness on the oxide scale formation on MCrAlY coatings studied in situ by high temperature X-ray diffraction.* Surface and Coatings Technology, 1998. **108-109**(1-3): p. 36-42.
145. Nijdam, T.J., L.P.H. Jeurgens, and W.G. Sloof, *Modelling the thermal oxidation of ternary alloys--compositional changes in the alloy and the development of oxide phases.* Acta Materialia, 2003. **51**(18): p. 5295-5307.
146. Wang, G., B. Gleeson, and D.L. Douglass, *A diffusional analysis of the oxidation of binary multiphase alloys.* Oxidation of Metals, 1991. **35**(5): p. 333-348.
147. Nijdam, T., C. Kwakernaak, and W. Sloof, *The effects of alloy microstructure refinement on the short-term thermal oxidation of NiCoCrAlY alloys.* Metallurgical and Materials Transactions A, 2006. **37**(3): p. 683-693.
148. Pike, L.M., Y.A. Chang, and C.T. Liu, *Solid-solution hardening and softening by Fe additions to NiAl.* Intermetallics, 1997. **5**(8): p. 601-608.
149. Yu, H.-C., A.V.d. Ven, and K. Thornton, *Theory of grain boundary diffusion induced by the Kirkendall effect.* Applied Physics Letters, 2008. **93**(9): p. 091908.
150. Gao, W. and Z. Li, *Nano-structured alloy and composite coatings for high temperature applications.* Materials Research, 2004. **7**: p. 175-182.
151. Dragos, U., et al., *Improvement of the oxidation behaviour of electron beam remelted MCrAlY coatings.* Solid State Sciences, 2005. **7**(4): p. 459-464.
152. Choi, H., et al., *Isothermal oxidation of air plasma spray NiCrAlY bond coatings.* Surface and Coatings Technology, 2002. **150**(2-3): p. 297-308.
153. Leyens, C., I.G. Wright, and B.A. Pint, *Effect of Experimental Procedures on the Cyclic, Hot-Corrosion Behavior of NiCoCrAlY-Type Bondcoat Alloys.* Oxidation of Metals, 2000. **54**: p. 255-276.
154. Tolpygo, V.K., D.R. Clarke, and K.S. Murphy, *Oxidation-induced failure of EB-PVD thermal barrier coatings.* Surface and Coatings Technology. **146-147**: p. 124-131.
155. Patterson, T., et al., *Thermal cyclic lifetime and oxidation behavior of air plasma sprayed CoNiCrAlY bond coats for thermal barrier coatings.* Surface and Coatings Technology, 2008. **203**(5-7): p. 437-441.
156. Ajdelsztajn, L., et al., *Synthesis and oxidation behavior of nanocrystalline MCrAlY bond coatings.* Journal of Thermal Spray Technology, 2005. **14**(1): p. 23-30.
157. He, J. and J.M. Schoenung, *Nanostructured coatings.* Materials Science and Engineering A, 2002. **336**(1-2): p. 274-319.
158. Li, C.-J. and W.-Y. Li, *Effect of sprayed powder particle size on the oxidation behavior of MCrAlY materials during high velocity oxygen-fuel deposition.* Surface and Coatings Technology, 2003. **162**(1): p. 31-41.

159. Itoh, Y., M. Saitoh, and M. Tamura, *Characteristics of MCrAlY Coatings Sprayed by High Velocity Oxygen-Fuel Spraying System.* Journal of Engineering for Gas Turbines and Power, 2000. **122**(1): p. 43-49.
160. Zhou, F., et al., *Microstructural evolution during recovery and recrystallization of a nanocrystalline Al-Mg alloy prepared by cryogenic ball milling.* Acta Materialia, 2003. **51**(10): p. 2777-2791.
161. Jiang, H.G., M.L. Lau, and E.J. Lavernia, *Grain growth behavior of nanocrystalline Inconel 718 and Ni powders and coatings.* Nanostructured Materials, 1998. **10**(2): p. 169-178.
162. Clemens, D., et al., *TEM and SNMS studies of protective alumina scales on NiCrAlY-alloys.* Fresenius' Journal of Analytical Chemistry, 1996. **355**(5): p. 703-706.
163. Fritscher, K., et al., *Kaysser Microscopy of Oxidation 3*. 1997, London: The Institute of Metals. 352.
164. Mercier, D., G. Kim, and M. Brochu, *Parameters influencing the oxidation behaviour of nanostructured CoNiCrAlY.* Paper submitted, 2009.